ANALYTICAL TRANSFORMATION PROPERTIES
OF LOSSLESS HYBRID T JUNCTIONS AND
ITS APPLICATION TO COMPLEX CONJUGATED
IMPEDANCE MATCHING

Sujeet K. Chaudhuri

A Thesis
in
Electrical Engineering

Presented to the Faculty of Graduate Studies and Research of the
University of Manitoba
in Partial Fulfillment of the Requirements for the
Degree of Master of Science

1972

ABSTRACT

The properties of symmetrical 4-port microwave junctions are considered. The symmetries of such 4-port junctions may be utilized to effect a reduction to an equivalent network consisting of junctions with two-ports interconnected by a network of ideal transformers. A virtue of this presentation is that it allows one to trace incident and reflected waves through the internal structure of the original junction. Employing the scattering matrix representation, the matching criteria for the case of generalized lossless matching two-ports are introduced and thus ultimately an analytical closed form solution of the impedance transformation loci is derived. Since in practice it is almost impossible to manufacture ideally symmetrical E - H junctions, both the theoretical (ideally symmetrical) and the practical (slightly asymmetrical) cases are treated separately. Transformation loci for E - H junction are plotted theoretically as well as experimentally. Furthermore an automated electronic tuning device (general outline only) is suggested with the help of the analytical transformation properties of the E - H tuner.

ACKNOWLEDGEMENTS

I wish to acknowledge my deep sense of gratitude and indebtedness to Dr. W. M. Boerner for suggesting the topic and for his valuable guidance. His constant encouragement, devoting a great deal of his time in supervising the work and giving suggestions, has enabled me to complete this work successfully.

I wish to express my appreciation for the financial support of the "National Research Council of Canada" (Grant No. A7240), without whose help, it would have been impossible to complete this research.

The computation work was performed with the facilities of the University of Manitoba Data Processing Centre.

I acknowledge with pleasure my debt to Miss Janet McKone for the care she has bestowed in doing the proof reading.

I would like to thank Mrs. Shirley Clubine for her skillful typing of the final version of the thesis.

In short, the entire host of my study colleagues and friends must be commended for their continuous encouragement and support which provided an essential stimulus for the development of this thesis.

Sujeet Chaudhuri

TABLE OF CONTENTS

LIST OF FIGURES

LIST OF SYMBOLS

Greek Alphabet:

α_1	$= \psi_{3_M} + \psi_{4_M}$ } For E - H tuner.
α_2	$= \psi_{3_M} - \psi_{4_M}$
α_3, α_4	Factors responsible for losses due to wear of the stub guide walls in E and H arms.
β	Imaginary part of the propagation constant.
ν	Complex propagation constant.
Δ	Perturbation in coupling of "3-db Coupler" (perfectly matched).
Δ_1, Δ_2	Perturbation in coupling of "3-db Coupler" (imperfect matching)
Δ'	Average of the two perturbations Δ_1 and Δ_2.
Δ''	$\frac{\Delta_2 - \Delta_1}{2}$.
ψ	Phase of the reflection coefficient Γ.
ψ_3	Transformation angle corresponding to ℓ_3. (in Appendix II used as phase angle corresponding to the reflection coefficient Γ_3).
ψ_4	Transformation angle corresponding to ℓ_4. (in Appendix II used as phase angle corresponding to the reflection coefficient Γ_4).
ψ_{2_M}	Phase of the reflection coefficient Γ_{2_M}.
ψ_{3_M}	Value of the transformation angle ψ_3 for which the load side reflection coefficient Γ_{2_M} is matched.
ψ_{4_M}	Value of the transformation angle ψ_4 for which the load side reflection coefficient Γ_{2_M} is matched.
$\sigma_{\mu\nu}$	Four-port scattering coefficient of the perturbed case. (μ = 1,2,3,4 & ν = 1,2,3,4).

$\bar{\sigma}_{22}$	Mean of σ_{11} and σ_{22}.
$\delta_{\mu\nu}$	Asymmetrical phase of scattering coefficient $\delta_{\mu\nu}$ because of perturbation (μ = 1, 2,3,4 & ν = 1,2,3,4).
$\phi_{\mu\nu}$	Phase angle of scattering coefficient $\delta_{\mu\nu}$ of four-port (μ = 1,2,3,4 & ν = 1,2,3,4).
$\lvert\phi_{2_M}\rvert$	$= \lvert \text{arc cos}(\lvert\Gamma_{2_M}\rvert)\rvert$.
$\lvert C_{\phi_{2_M}}\rvert$	The circle defined as $\lvert\phi_{2_M}\rvert = \text{arc cos}(\lvert\Gamma_{2_M}\rvert)$.
λ_g	Guide wave length.
Γ_1	Input reflection coefficient (plane 1).
Γ_2	Load reflection coefficient (plane 2).
Γ_3	Reflection coefficient corresponding to locus ψ_3 = const.
Γ_4	Reflection coefficient corresponding to locus ψ_4 = const.
Γ_r	Real part of Γ_{2_M}.
Γ_i	Imaginary part of Γ_{2_M}.

Latin Alphabet:

L_3	Circular loci when ψ_3 = const.; ψ_4 = adjustable.
L_4	Circular loci when ψ_4 = const.; ψ_3 = adjustable.
ℓ_3	Geometrical length of E arm.
ℓ_4	Transformation length of H arm.
$s_{11}, s_{12}, s_{21}, s_{22}$	Scattering coefficients of the equivalent two-port junction.
s_{55}, s_{66}	Internal reflection coefficients of E or H arm.

Z_{in}	Input impedance.
Z_L	Normalized complex load impedance.
$[S_H]$	Equivalent two-port scattering matrix.
$[E]$	Diagonal identity matrix.
$\delta_{\mu\nu}$	Scattering coefficient of four-port junction ($\mu = 1,2,3,4$ & $\nu = 1,2,3,4$).

Chapter 1

1.1 INTRODUCTION

The ultimate aim is to derive an analytical closed form solution of the impedance transformation loci of various microwave junctions and to use it for the design of automatic tuners.

The concept of complex conjugated impedance matching (Megla,1961) is briefly broached in context with the basic approach to the problem. Consider Fig.1, (which represents the gross simplified equivalent circuit of the principal set-up as shown in Fig.2). Here V_o denotes the open-circuited voltage of the generator, $Z_g = R_g + jX_g$ the lumped generator impedance at the input transformation plane of the linear device, and $Z_L = R_L + jX_L$ the transformed load impedance of the entire linear microwave device. Since the load current may be defined as $I_L = V_o(Z_g + Z_L)^{-1}$, the received real load power is given by

$$P_L = 1/2 \; \mathrm{Re}\{I_L V_L^*\} = \frac{V_o^2 \; R_L}{2(Z_g+Z_L)(Z_g+Z_L)^*} \qquad (1.1.1a)$$

where the superscript * denotes the complex conjugated quantity.

Maximum real power is transferred if the optimization conditions $\frac{\partial}{\partial R_L}(P_L) = 0$ and $\frac{\partial}{\partial X_L}(P_L) = 0$ are satisfied subject to the condition that $R_L \neq 0$, i.e.

$$R_g = R_L \quad \text{and} \quad X_g = -X_L \quad \text{or} \quad Z_g = Z_L^* \qquad (1.1.1b)$$

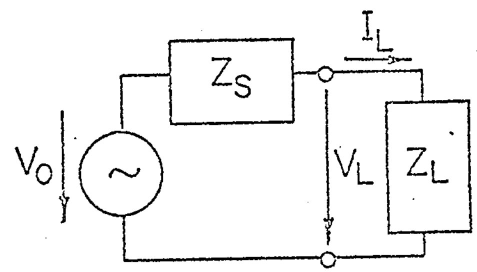

Figure I Simplified Equivalent Circuit

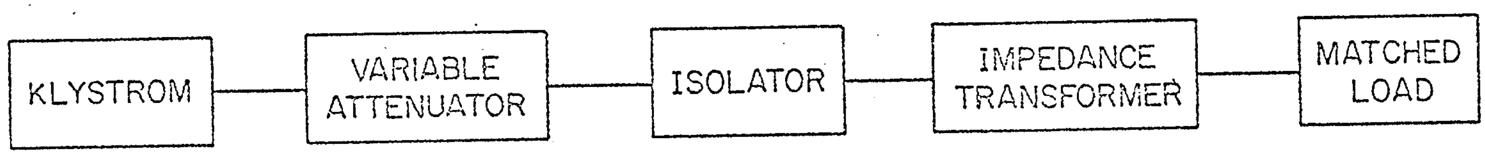

Figure 2 Principal Measurement Set-up

Assuming that a critical maximum of the load power is obtained from known power-dependent changes of the linear device, the input impedance of the entire non-linear device can then be precisely determined from the matching condition (1.1.1b) if the transformation properties of the tunable lumped generator impedance are known (Boerner, 1963). To employ the concept of complex conjugated impedance matching at extremely low power densities, it is sufficient to isolate the load-dependent generator impedance (Altschuler,1962) and to cascade an impedance transformer between the isolated generator and the load so that the generator side input impedance of the transformer is matched to the characteristic waveguide impedance as is shown in Fig.2. Since it is anticipated that the output impedance of the impedance transformer may require any possible passive value to match the conjugated transformed load impedance, the transformation junction must be designed such that the entire passive impedance can be transformed.

A microwave device for which it is known that it satisfies these transformation properties is the lossless hybrid T junction of Fig.3. The illustrated E-H junction is a commonly employed immittance transformer in microwave technology and it consists of a symmetrical series (E-arm) - parallel (H arm) - junction of rectangular waveguides with identical cross-sections which are operated in the fundamental TE_{10} mode (Montgomery and Griesheimer,1947). In particular, it is assumed that the junction is isotropic and lossless and that the design is geometrically symmetric, i.e. the E and H arms have a common symmetry plane about which the transformation planes 1 and 2 are symmetrically spaced as is indicated in Fig.3. Under these idealized assumptions, the E and H arms are decoupled (Stösser,1961) as is verified by the unitarity conditions derived in Appendix I, where the slightly asymmetrical design case is treated as well.

In applying the E - H junction as an immittance transformer, the H(3) and E(4) arms are terminated in tunable short-circuited plungers and by proper choice of the equivalent transformation lengths ℓ_3 and ℓ_4 from the central symmetry planes, it is possible to transform the load dependent reflection coefficient Γ_2 (plane 2) into the input reflection coefficient $\Gamma_1 = 0$ (plane 1) as defined in Fig.4. In practice, the transformation problem is solved by either measuring Γ_1, employing directional couplers, or by measuring the absorbed maximum power P_L of the load device by changing ℓ_3 and ℓ_4 until $\Gamma_1 = 0$ or $P_L = P_{max}$. The exact functional dependence of Γ_2 on ℓ_3, ℓ_4 and the design parameters of the hybrid junction may commonly be of little interest to the experimentalist, though the transformation behaviour is known to be highly non-uniform in the case of unmatched E - H tuners (Sucher and Fox, 1963). However, if the hybrid T junction is to be employed as an automated, controllable impedance transformer in a measurement procedure based on the principle of complex conjugated impedance matching, the analytical transformation properties must be defined in a closed form mathematical representation in dependence of the scattering parameters of the four-port as derived in *Chapter 3*.

To properly analyze the transformation properties of symmetrical E - H

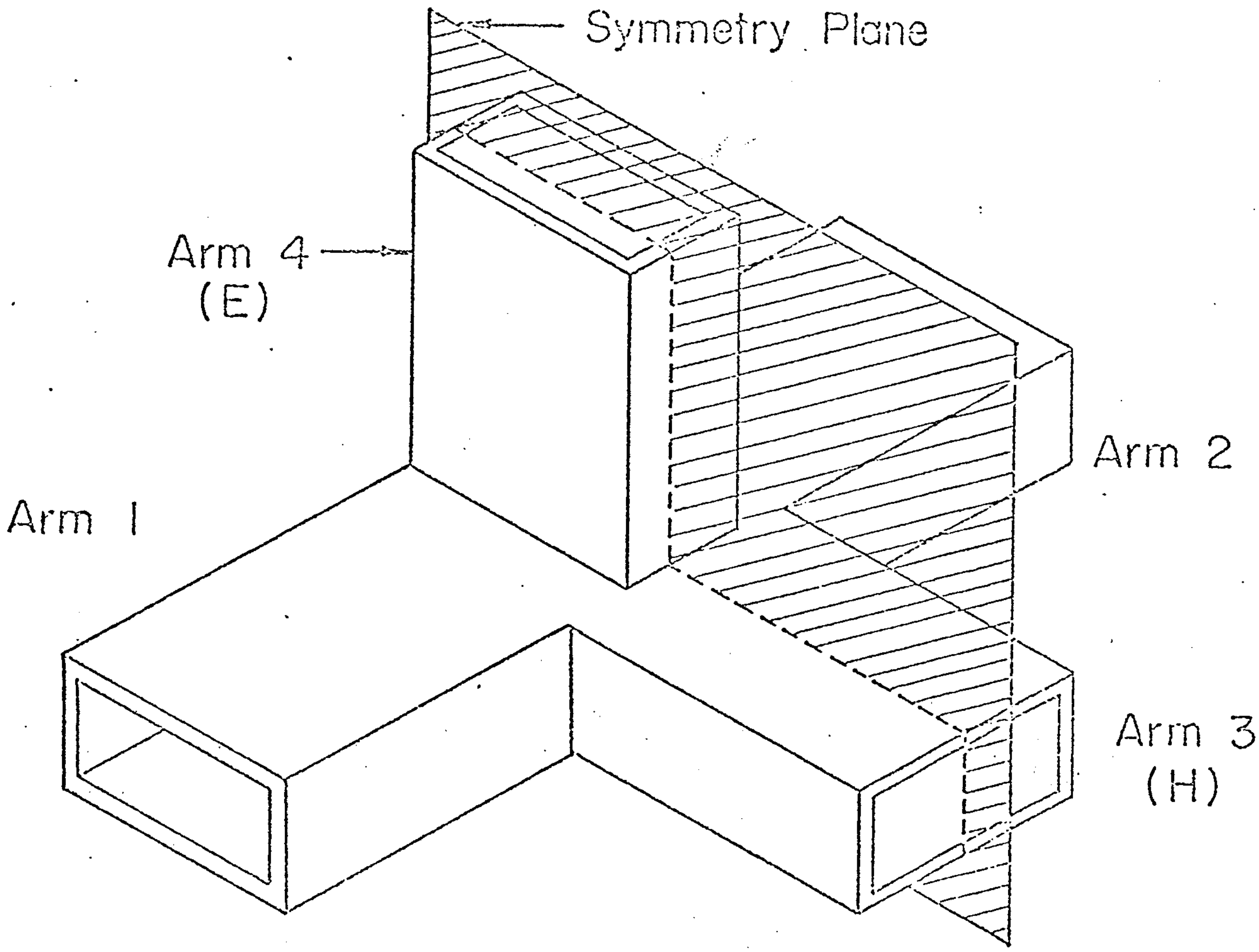

Fig. 3 Symmetrical E-H T JUNCTION

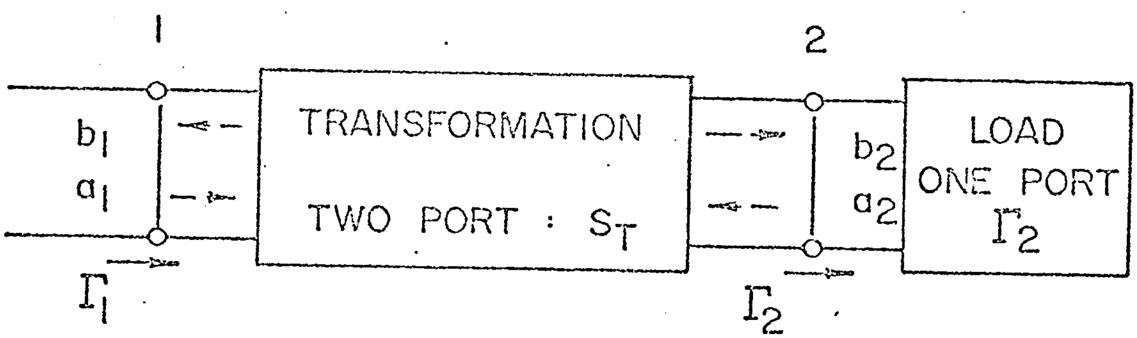

Fig. 4 Equivalent Transformation Two-Port

tuners, the properties of various symmetrical designs have been determined by measurement. Measurement procedures as described in detail (*Chapter 5*) and illustrated in the self-explanatory Fig.5, have been employed using the Owens' method (Owens, 1969) to increase the measurement accuracy in regions of high VSWR. Measurement data compiled in *Chapter 5* for symmetrical E - H tuners show that if port 1 or 2 is matched and one of the tunable short-circuited plungers is held on fixed position whereas the other stub is moved over one-half wavelength and vice versa, circular transformation loci for the input impedance results at port 2 or 1, respectively. Neglecting the slight losses, it is found that any one of these transformation loci intersects the matching point, i.e. $\Gamma = S_{22} = 0$, and all loci are tangent to the unit mismatch circle, i.e. $|\Gamma| = 1$, as is shown in Fig.6a. Thus two families of circular transformation loci result in the Smith Chart, i.e. locus $L_3(\ell_3 =$ const., $\ell_4 =$ turnable) whose intersection point defines the load-side reflection coefficient $S_{22} = \Gamma_2^*$ as shown in Fig.6b. In particular, it is found that for the lossless case the entire passive region of the impedance plane can be transformed if the E and H arms are decoupled and not entirely mismatched in which case the two families of circular loci are explicitly independent of one another.

In order to analyze these experimental results, the matching criteria for a generalized lossless reciprocal matching two ports are given in *Chapter 2*, employing the scattering matrix approach (Carlin and Giordano,1964). Although the general properties of hybrid T junctions are rather well established in the literature (Kahn, Oono,...1956;

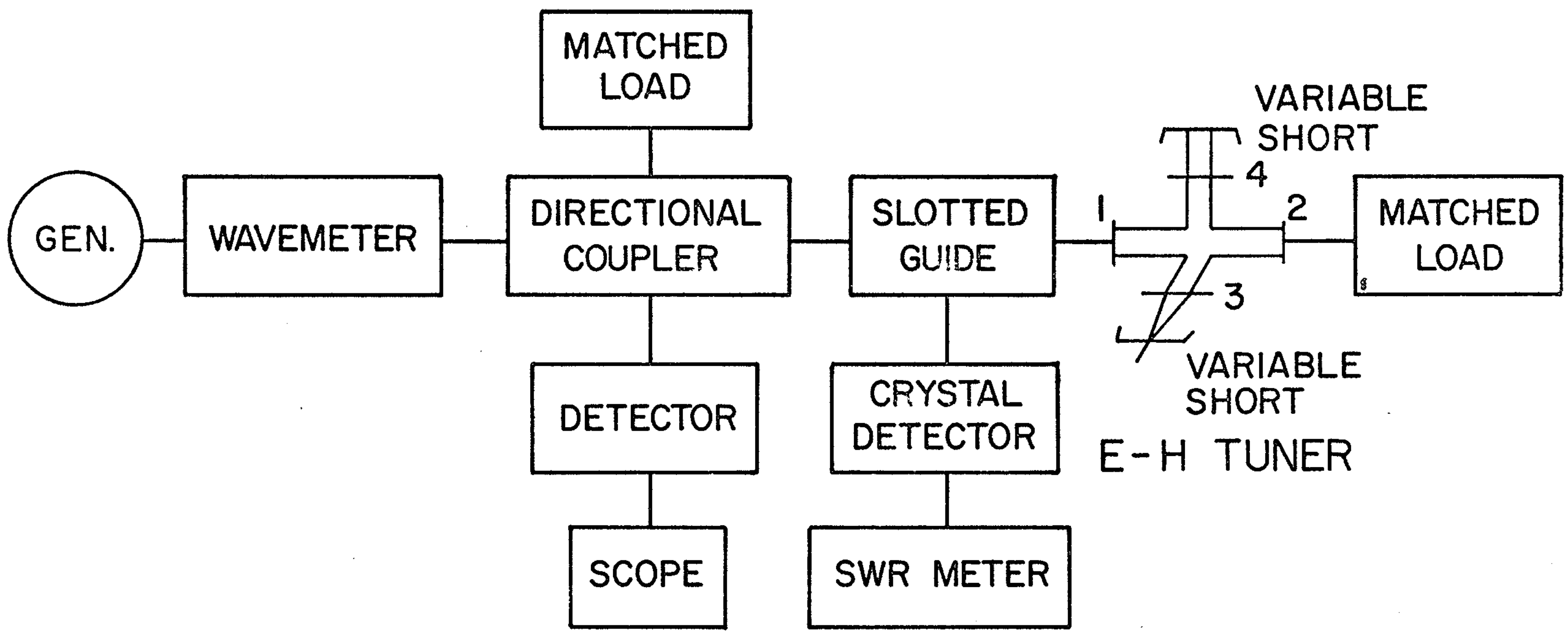

Fig. 5 Measurement Set-Up

Fig. 6. a. Polar Representation of $\phi_{2M} = \arc\cos(|\Gamma_{2M}|)$

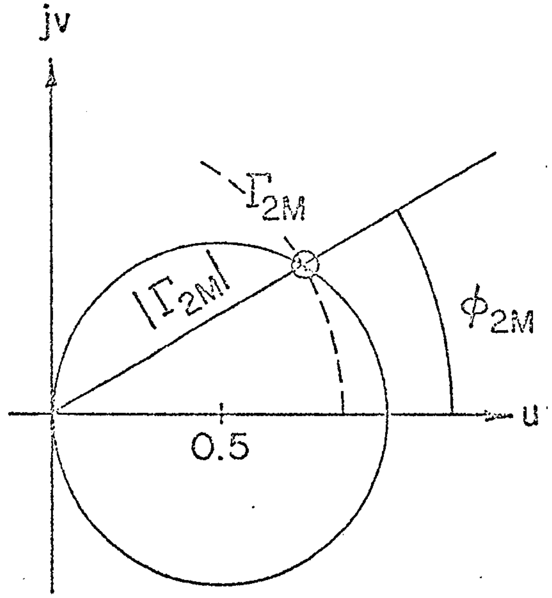

Fig. 6. b. Graphical Evaluation

$\psi_{3M} = \psi_{2M} (\pm) |\psi_{2M}|$

$\psi_{4M} = -\psi_{2M} (\mp) |\phi_{2M}|$

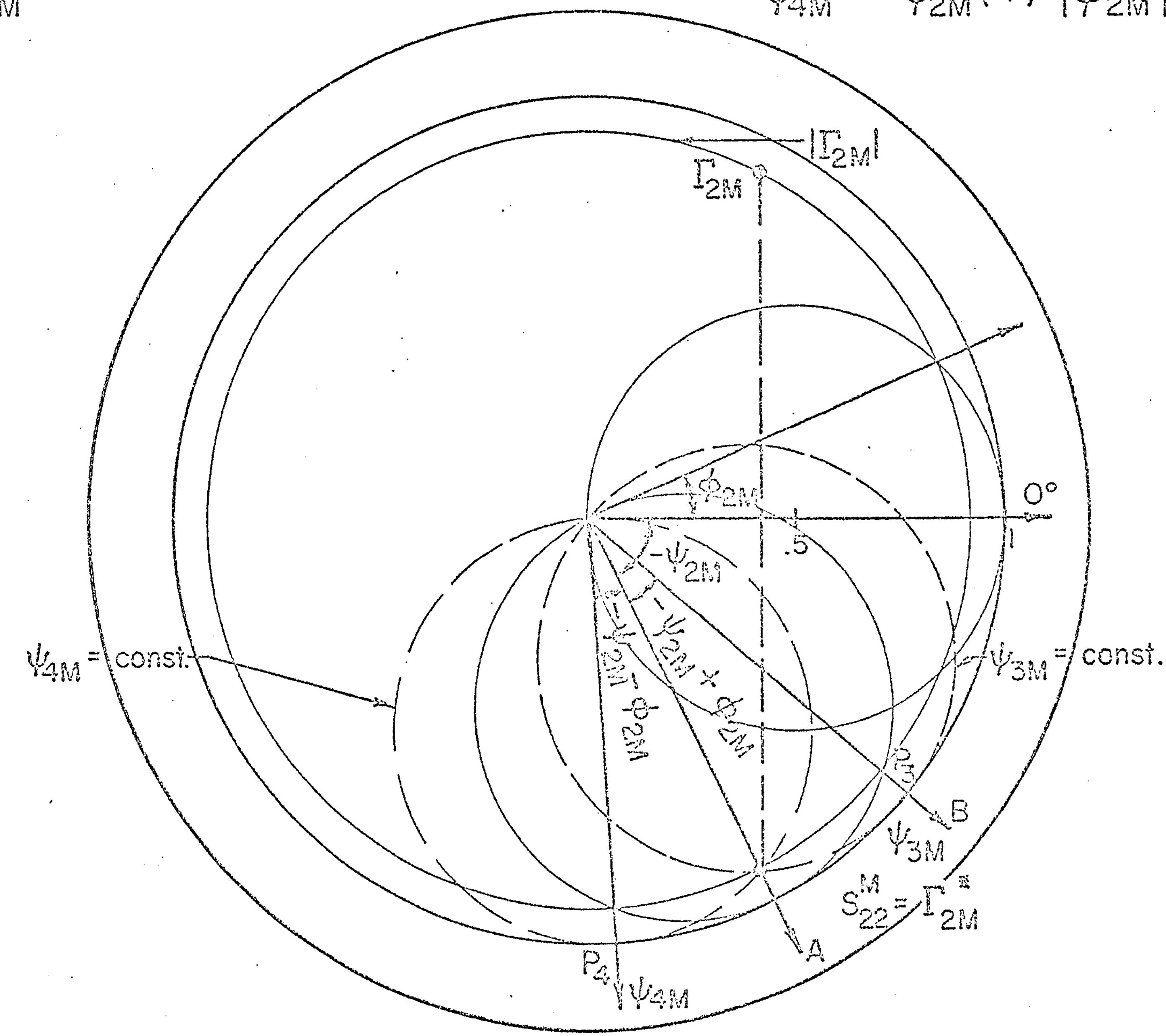

Brand,1969), the unitary properties are carefully reviewed in Appendix I. The resulting identities are then employed in *Chapter 3* and in *Chapter 4* respectively, to define the general expression for the reflection coefficient $S_{22} = \Gamma_2^*$ of isotropic, lossless, symmetrical (as well as slightly asymmetrical) hybrid T junction and '3-db short slot' directional coupler. Based on the analysis of *Chapter 3*, the analytical transformation equations required for conjugate impedance matching are established in *Chapter 6*. Both the matching conditions of defining the stub lengths ℓ_3 and ℓ_4 for a given $\Gamma_2^* = S_{22}$ and of determining $\Gamma_2 = S_{22}^*$ for known stub lengths ℓ_3 and ℓ_4 are derived. The detailed analysis of the closed form solution of the intersecting impedance transformation loci presented in *Chapter 6* was not found in the literature. In addition, the analysis of matching errors due to slightly coupled E and H arms as well as losses in the tunable stubs seem to be novel to the best of the author's knowledge.

These properties are effectively applied in *Chapter 7* to general design problems of automated and controllable input power matching devices. How these properties can be used in general design problems of microwave technology is summarized in the conclusions.

Chapter 2

MATCHING CRITERIA FOR LOSSLESS TWO-PORTS

AND

REDUCTION FROM FOUR-PORT TO TWO-PORT JUNCTION.

2.1 MATCHING CRITERIA FOR LOSSLESS TWO-PORTS

Since the ultimate aim is to derive an analytical closed form solution of the impedance transformation loci, the matching criteria for the case of generalized lossless matching two-ports are introduced employing the scattering matrix representation (Carlin, Oono, Kahn, Belevitch, 1956). Using these criteria, it must be shown that for a given symmetrical hybrid T junction an arbitrary load side reflection coefficient Γ_2 for which $|\Gamma|<1$ can be transformed in all cases into $\Gamma_1 = 0$.

The symmetrical hybrid T junction whose decoupled E & H arms are terminated in tunable short-circuited plungers, may be considered a lossless two-port between the transformation planes 1 & 2. In Fig.4, the equivalent two-port configuration is presented, where the associated scattering matrix is defined by

$$[B_T] = [S_T]\ [A_T] \tag{2.1.1a}$$

with

$$[B_T] = \begin{bmatrix} b_1 \\ b_2 \end{bmatrix},\ [A_T] = \begin{bmatrix} a_1 \\ a_2 \end{bmatrix},\ [S_T] = \begin{bmatrix} S_{11} & S_{12} \\ S_{21} & S_{22} \end{bmatrix} \tag{2.1.1b}$$

and

$$a_2 = \Gamma_2 b_2,\quad b_1 = \Gamma_1 a_1 \tag{2.1.1c}$$

The input reflection coefficient Γ_1 resulting from the cascaded transformation two-port and the load one-port thus becomes (Carlin and Giordano, 1964).

$$\Gamma_1 = S_{11} + \frac{\Gamma_2 \cdot S_{12}S_{21}}{1 - \Gamma_2 S_{22}} = \frac{S_{11} - \Gamma_2 \cdot \mathrm{Det}\{[S_T]\}}{1 - \Gamma_2 S_{22}} \tag{2.1.2}$$

which must vanish for matching conditions. Assuming that the two-port is lossless, the scattering matrix must be para-unitary (Carlin, 1956), i.e.

$$|S_{11}|^2 + |S_{21}|^2 = 1 \tag{2.1.3a}$$

$$|S_{22}|^2 + |S_{12}|^2 = 1 \tag{2.1.3b}$$

$$S_{11}^* S_{12} + S_{21}^* S_{22} = 0 \tag{2.1.3c}$$

where $S_{\mu\nu}^*$ denotes the complex conjugate of $S_{\mu\nu}$. For a lossless, reciprocal two-port the following conditions follow from (2.1.3)

$$\mathrm{Det}\,\{[S_T]\} = \frac{S_{22}}{S_{11}^*}, \quad |S_{11}| = |S_{22}|$$

$$\text{and} \qquad |S_{12}| = |S_{21}| \tag{2.1.4}$$

If conditions (2.1.3) and (2.1.4) are resubstituted into (2.1.2), it is found that the input reflection coefficient of a lossless reciprocal two-port reduces to

$$\Gamma_1 = \frac{S_{22}}{S_{11}^*} \cdot \frac{S_{22}^* - \Gamma_2}{1 - \Gamma_2 S_{22}} \tag{2.1.5a}$$

resulting in the following matching criterior

$$\Gamma_2 = S_{22}^*, \quad |\Gamma_2| \neq 1 \tag{2.1.5b}$$

which is a necessary and sufficient condition for a lossless, reciprocal matching transformer. Furthermore, condition (2.1.5b) satisfies condition (1.1.1b), i.e. complex conjugated impedance matching, where the criteria for matching any arbitrary passive load impedance, i.e. $|\Gamma_2|<1$, follows directly from (2.1.5b) and is given by

$$0 < |S_{22}| < 1 \qquad (2.1.6a)$$

$$0 < \mathrm{Arc}(S_{22}) \leq 2\Pi \qquad (2.1.6b)$$

It is well known that the transformation condition (2.1.6) is not satisfied by many of the commonly employed microwave devices (Kahn, 1956) and only a restricted domain of Γ_2 can be transformed, e.g. double-stub matching. Thus it will be shown that the lossless, symmetrical E-H tuner and 3 - db coupler do, in general, satisfy condition (2.1.6).

2.2 REDUCTION FROM FOUR-PORT TO TWO-PORT JUNCTION

To determine the restriction on the transformation properties of hybrid T junctions, the two-port scattering parameters $S_{\mu\nu}$ as defined in Fig.4 must be expressed in terms of the scattering four-port parameters $S_{\mu\nu}$. Therefore, the equivalent transformation circuit of the hybrid four-port as defined in Fig.7 is introduced, where the tunable short circuited sections of the E and H arm one-ports are combined into a separate two-port defined by

$$[B_S] = [S_S]\ [A_S] \qquad (2.2.1a)$$

with

$$[A_S] = \begin{bmatrix} a_5 \\ a_6 \end{bmatrix} \quad \text{and} \quad [B_S] = \begin{bmatrix} b_5 \\ b_6 \end{bmatrix} \qquad (2.2.1b)$$

Since the E and H arms are adjusted independently, the E and H arm one-ports are decoupled, i.e. $S_{56} = S_{65} = 0$, and therefore

$$[S_S] = \begin{bmatrix} S_{55} & 0 \\ 0 & S_{66} \end{bmatrix} \qquad (2.2.1c)$$

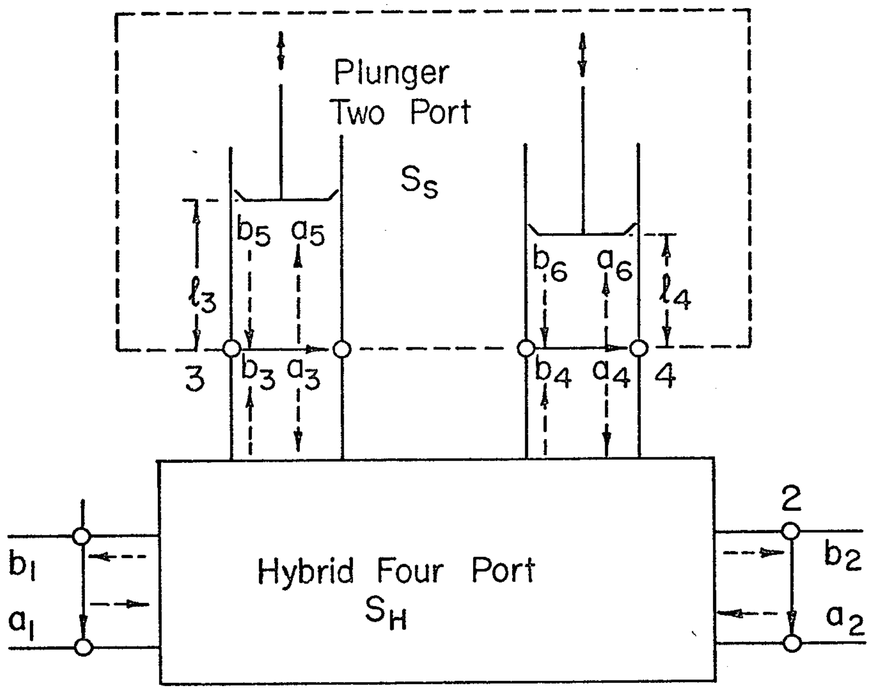

Fig. 7 Shunting of Hybrid Four Ports with Short-Circuited Plunger Two Ports

Although, for all practical design reasons, it may be assumed that the waveguide junction itself is lossless, the losses due to imperfectly tuned shorts as well as those due to wear of the stub guide walls must be considered in the definition of S_{55} and S_{66}. These internal one-port reflection coefficients are straightforwardly obtained from transmission line theory (King,1965), where it is assumed that the waveguide sections of the respective stubs and arms are matched to a common characteristic impendance. The normalized one-port input impedance may therefore be defined as

$$Z_{in} = \frac{Z_L + \tanh\gamma\ell}{1 + Z_L\tanh\gamma\ell} = \frac{\tanh u + \tanh v}{1 + \tanh u \tanh v} = \tanh(u+v) \qquad (2.2.1d)$$

Where $Z_L = \tanh v$ represents the normalized complex load impedance of the tunable short, and $\gamma = v/\ell = \alpha + j\beta$ the complex propagation constant with α the attenuation constant and β the phase constant of the stub guide section.

The internal reflection coefficient $S_{\mu\mu}$ ($\mu = 5,6$) is thus given by

$$S_{\mu\mu} = \frac{Z_{in_\mu} - 1}{Z_{in_\mu} + 1} = \frac{\tanh(u+v)_\mu - 1}{\tanh(u+v)_\mu + 1} = -\exp{-2(u+v)_\mu} \qquad (2.2.1e)$$

which for the lossless case reduces to

$$S_{\mu\mu} = -\exp{-2j\beta_\mu\ell_\mu} = -\exp{-2j\phi_\mu} \qquad (2.2.1f)$$

The formulation of the scattering matrix $[S_H]$ of the equivalent four-port hybrid T junction is based on the assumption that the material constituents are isotropic, implying reciprocity (Carlin & Giordano, 1964), i.e. $S_{\mu\nu} = S_{\nu\mu}$ and therefore

$$[S_H] = [S_H]^T \tag{2.2.2a}$$

where the superscript T denotes matrix transposition.

Furthermore, it is assumed that the losses of the hybrid T junction are negligible and therefore $[S_H]$ must satisfy the unitarity condition (Carlin & Giordano, 1964),i.e.

$$[S_H]^{*T}\,[S_H] = [E] \tag{2.2.2b}$$

where [E] is a diagonal identity matrix. Without introducing symmetry conditions and employing the wave definitions of Fig. 7, the following results;

$$\begin{bmatrix}[B_T]\\[B_A]\end{bmatrix} = \begin{bmatrix}S_H\end{bmatrix}\cdot\begin{bmatrix}[A_T]\\[A_A]\end{bmatrix} = \begin{bmatrix}[Q] & [T]\\ [T]^T & [R]\end{bmatrix}\cdot\begin{bmatrix}[A_T]\\[A_A]\end{bmatrix} \tag{2.2.3a}$$

where

$$[A_T] = \begin{bmatrix}a_1\\a_2\end{bmatrix},\ [B_T] = \begin{bmatrix}b_1\\b_2\end{bmatrix} \text{ and } [A_A] = \begin{bmatrix}a_3\\a_4\end{bmatrix},[B_A]=\begin{bmatrix}b_3\\b_4\end{bmatrix} \tag{2.2.3b}$$

The submatrices [Q], [T], its transposes $[T]^T$ and [R] are defined with (2.2.2) and (2.2.3) by

$$[Q] = \begin{bmatrix}s_{11} & s_{12}\\ s_{12} & s_{22}\end{bmatrix},[T] = \begin{bmatrix}s_{13} & s_{14}\\ s_{23} & s_{24}\end{bmatrix}\text{and}[R] = \begin{bmatrix}s_{33} & s_{34}\\ s_{34} & s_{44}\end{bmatrix} \tag{2.2.3c}$$

The desired scattering matrix $[S_T]$ of the equivalent transformation two-port, as defined by (2.1.1a) and in Fig.4, can be obtained from (2.2.3a), where

$$[B_T] = [Q][A_T] + [T][A_A] \tag{2.2.4a}$$

$$[B_A] = [T]^T[A_T] + [R][A_A] \tag{2.2.4b}$$

However, since at the transformation planes 3 and 4 the following identities must be satisfied according to the definition of Fig.7.

$$[A_A] = [B_S] \quad \text{and} \quad [B_A] = [A_S] \tag{2.2.5a}$$

it follows that $[A_A] = [S_S][B_A]$ or

$$[B_A] = [S_S]^{-1}[A_A] \tag{2.2.5b}$$

Substituting (2.2.5b) into (2.2.4b) and solving for $[A_A]$ yields

$$[A_A] = \{[S_S]^{-1} - [R]\}^{-1} \cdot [T]^T[A_T] \tag{2.2.5c}$$

which when substituted into (2.2.4a), results in the desired formulation of the scattering matrix $[S_T]$ defined in (2.1.1a)

$$[S_T] = \{[Q] + [T] \cdot \{[S_S]^{-1} - [R]\}^{-1}[T]^T\} \tag{2.2.6a}$$

where with $D = \{(\frac{1}{s_{55}} - s_{33})(\frac{1}{s_{66}} - s_{44}) - s_{34}^2\}$

$$S_{11} = s_{11} + \{s_{13}^2(\frac{1}{s_{66}} - s_{44}) + 2s_{13}s_{14}s_{34} + s_{14}^2(\frac{1}{s_{55}} - s_{33})\}\frac{1}{D} \tag{2.2.6b}$$

$$S_{12} = S_{21} = s_{12} + \{s_{13}s_{23}(\frac{1}{s_{66}} - s_{44}) - s_{34}(s_{14}s_{23} + s_{13}s_{24}) + s_{14}s_{24}(\frac{1}{s_{55}} - s_{33})\}\frac{1}{D} \tag{2.2.6c}$$

$$S_{22} = s_{22} + \{s_{23}^2(\frac{1}{s_{66}} - s_{44}) + 2s_{23}s_{24}s_{34} + s_{24}^2(\frac{1}{s_{55}} - s_{33})\}\frac{1}{D} \tag{2.2.6d}$$

Since in practice it is almost impossible to manufacture ideally symmetrical E-H tuners, both the theoretical (ideally symmetrical) and the practical (slightly asymmetrical) cases are treated separately in the following chapter, utilizing the unitarity identity derived in Appendix I.

Chapter 3

HYBRID T-JUNCTION TUNERS

3.1 IDEALLY SYMMETRICAL E-H TUNERS

If it is assumed that the properties of the E-H junction is geometrically symmetric i.e. the E and H arms have a common symmetry plane about which the transformation planes 1 and 2 are symmetrically spaced and no dents or obstacles are perturbing the fields in the junction, then the symmetry conditions given in (I-7) must be satisfied, i.e. $s_{22} = s_{11}$, $s_{23} = s_{13}$, $s_{24} = -s_{14}$ and $s_{34} = 0$, where $s_{33} \neq 0$ and $s_{44} \neq 0$ for an unmatched symmetrical E-H tuner.

Subject to these conditions, it is found that the equivalent two-port is symmetric, where

$$s_{11} = s_{22} = S_{11} + \frac{S_{13}^2}{1/S_{55}-S_{33}} + \frac{S_{14}^2}{1/S_{66}-S_{44}} \tag{3.1.1a}$$

and

$$s_{12} = s_{21} = S_{12} + \frac{S_{13}^2}{1/S_{55}-S_{33}} - \frac{S_{14}^2}{1/S_{66}-S_{44}} \tag{3.1.1b}$$

substituting expressions (I-9a) and (I-9b) for s_{11} and s_{12}, respectively, a more convenient representation of the two-port scattering parameters is found.

$$s_{11} = s_{22} = \frac{1}{2}\,\frac{S_{13}}{S_{13}^*}\,\frac{[1-\frac{S_{33}^*}{S_{55}}]}{[1/S_{55}-S_{33}]} + \frac{1}{2}\,\frac{S_{14}}{S_{14}^*}\,\frac{[1-\frac{S_{44}^*}{S_{66}}]}{[1/S_{66}-S_{44}]} \tag{3.1.2a}$$

$$s_{12} = s_{21} = \frac{1}{2}\,\frac{S_{13}}{S_{13}^*}\,\frac{[1-\frac{S_{33}^*}{S_{55}}]}{[1/S_{55}-S_{33}]} - \frac{1}{2}\,\frac{S_{14}}{S_{14}^*}\,\frac{[1-\frac{S_{44}^*}{S_{66}}]}{[1/S_{66}-S_{44}]} \tag{3.1.2b}$$

Employing the notation $S_{\mu\nu} = |S_{\mu\nu}| \exp j\phi_{\mu\nu}$ and substituting the expressions of s_{55} and s_{66} as defined in (2.2.1f) for the purely lossless tuners, i.e. $S_{\mu\mu} = -\exp -2j\phi_{\mu}$, into (3.1.2a), yields with $\phi_{55} = \phi_3$ and $\phi_{66} = \phi_4$.

$$s_{22} = -\tfrac{1}{2}\{\exp j2(\phi_{13}-\phi_3)\frac{1+|S_{33}|\exp +j(2\phi_3-\phi_{33})}{1+|S_{33}|\exp -j(2\phi_3-\phi_{33})}$$

$$+ \exp j2(\phi_{14}-\phi_4)\ \frac{1+|S_{44}|\exp +j(2\phi_4-\phi_{44})}{1+|S_{44}|\exp -j(2\phi_4-\phi_{44})}\} \qquad (3.1.3a)$$

For further analysis it is convenient to define the zero-setting of the adjustable stubs $\ell_p = \ell_3$ and $\ell_s = \ell_4$ with respect to the fixed reference planes of the H and E arms so that

$$\phi_3' = \phi_3 - \frac{\phi_{33}}{2} \text{ and } \phi_4' = \phi_4 - \frac{\phi_{44}}{2} \qquad (3.1.3b)$$

which when substituted into (3.1.3a) results in

$$s_{22} = -\tfrac{1}{2}\{\exp j(\Theta_{13}-2\Theta_3(\phi_3', |S_{33}|)+\exp j(\Theta_{14}-2\Theta_4(\phi_4', |S_{44}|)\} \qquad (3.1.3c)$$

where Θ_{13} and Θ_{14} are defined by (I-10d) and (I-10e) of Appendix I, and

$$\Theta_{\mu} = \tan^{-1}\{\frac{1-|S_{\mu\mu}|}{1+|S_{\mu\mu}|}\tan\ \phi_{\mu}'\}, \qquad \mu = 3,\ 4 \qquad (3.1.3d)$$

Inspecting (3.1.3), it is obvious that for a lossless, symmetrical hybrid T junction the entire complex plane of the reflection coefficient $s_{22} = \Gamma_2^*$ can be transformed, as long as the short-circuited tuners are lossless, $|s_{33}|<1$ and $|s_{44}|<1$, and ϕ_3 and ϕ_4 are independently adjustable over the ranges $0\leq\phi_3\leq\pi$ and $0\leq\phi_4\leq\pi$.

Introducing the abbreviations

$$\psi_3(\phi_3 = \text{Const.}, \phi_4 \text{ adj}) = [\Theta_{14}-2\Theta_4(\phi_4', |s_{44}|)-\pi] \qquad (3.1.4a)$$

$$\Psi_4(\phi_4 = \text{Const.}, \phi_3 \text{ adj}) = [\Theta_{13} - 2\Theta_3(\phi_3', |s_{33}|) - \pi \qquad (3.1.4b)$$

(3.1.3c) can be then rewritten as

$$\begin{aligned} s_{22} &= \tfrac{1}{2}\{\exp j\psi_4 + \exp j\psi_3\} \\ &= \tfrac{1}{2}[\exp j(\tfrac{\psi_4-\psi_3}{2}) + \exp - j(\tfrac{\psi_4-\psi_3}{2})]\exp j(\tfrac{\psi_4+\psi_3}{2}) \qquad (3.1.4c) \\ &= \cos(\tfrac{\psi_3-\psi_4}{2})\exp j(\tfrac{\psi_3+\psi_4}{2}) = \Gamma_2^* \end{aligned}$$

The analytical transformation properties (3.1.4) as related to the concept of complex conjugated impedence matching are derived and interpreted in Chapter 6.

3.2 SLIGHTLY ASYMMETRICAL E-H TUNERS

Since in practice it is found that slight coupling of the transformation arms exists even for optimized designs, perfect symmetry can no longer be justified if the E-H tuner is to be employed as an accurate immittance matching device. Therefore, first order perturbations from the ideally symmetrical design case must be analyzed which represent either a slight shift of the E and H arm symmetry planes with respect to port 1 and 2 or a slight off-axis dent in the main junction, or angle of E or H arm plane different from 90° with respect to the main arm. Denoting the scattering coefficients of the perturbed case by $\sigma_{\mu\nu}$, and inspecting the symmetry constraints given in (I-5) and (I-6) of Appendix I, it is shown in (I-13) and (I-14) that a slight asymmetrical phase shift in the transformation coefficients σ_{13}, σ_{23}, σ_{14} and σ_{24} results in coupling of the transformation arms. Namely, if it is assumed that,

$$\sigma_{13} = S_{13}\exp j\delta_{13} \quad , \quad \sigma_{23}=S_{13}\exp j\sigma_{13}$$

$$\sigma_{14} = S_{14}\exp j\delta_{14} \quad , \quad \sigma_{24} = -S_{14}\exp -j\delta_{14} \tag{3.2.1a}$$

and

$$\sigma_{11} = S_{11}\exp j\delta_{11}, \quad \sigma_{12} = S_{12}, \quad \sigma_{22} = S_{11}\exp -j\delta_{11} \tag{3.2.1b}$$

then the coupling coefficient is finite for $s_{13} \neq s_{14}$, where

$$\sigma_{34} = -j\frac{S_{13}S_{14}\sin(s_{13}-s_{14})S^{*}_{11}\cos s_{11}}{[|S_{13}|^2\cos 2\delta_{13}-|S_{14}|^2\cos 2\delta_{14}]}, \quad S_{13}\neq S_{14} \tag{I-15a}$$

and σ_{33} and σ_{34} will change in modulus and phase as is shown in (I-15c) and (I-15d).

Employing these assumptions, the above stated perturbation requirements are satisfied and it is possible to obtain an estimate of the transformation error. In order to analyze the first order perturbation effects in the most general way, both the two port reflection coefficient σ_{22} and the mean $\bar{\sigma}_{22} = \frac{1}{2}(\sigma_{11} + \sigma_{22})$ are evaluated, where in terms of σ_{33}, σ_{34} and σ_{44}

$$\begin{aligned}\sigma_{22} = \{&S_{11}\exp -j\delta_{11}[(\frac{1}{S_{55}} -\sigma_{33})(\frac{1}{S_{66}} -\sigma_{44})-\sigma^2_{34}] \\ &+ S^2_{13}\exp(-2j\delta_{13})(1/S_{66}-\sigma_{44})+S^2_{14}\exp(-2j\delta_{14})(1/S_{55}-\sigma_{33}) \\ &- 2S_{13}S_{14}\exp -j(\delta_{13}+\delta_{14})\sigma_{34}\}\{(\frac{1}{S_{55}} -\sigma_{33})(\frac{1}{S_{66}} -\sigma_{44})-\sigma^2_{34}\}^{-1}\end{aligned} \tag{3.2.2a}$$

and

$$\begin{aligned}\bar{\sigma}_{22} = \tfrac{1}{2}(\sigma_{11}+\sigma_{22})=\{&S_{11}\cos\delta_{11}[(\frac{1}{S_{55}} -\sigma_{33})(\frac{1}{S_{66}} -\sigma_{44})-\sigma^2_{34}] \\ &+ S^2_{13}\cos 2\delta_{13}(1/S_{66}-\sigma_{44})+S^2_{14}\cos 2\delta_{14}(1/S_{55}-\sigma_{33}) \\ &+ 2jS_{13}S_{14}\sin(\delta_{13}+\delta_{14})\sigma_{34}\}\{(\frac{1}{S_{55}} -\sigma_{34})(\frac{1}{S_{66}} -\sigma_{44})-\sigma^2_{34}\}^{-1}\end{aligned} \tag{3.2.2b}$$

where σ_{33}, σ_{34}, σ_{44} and δ_{11} are defined in (I-15) and the modulus and phase constraints of the unperturbed scattering coefficients $S_{\mu\nu}$ are satisfied by the relations given in (I-8) to (I-12).

It is to be noted that it was found more convenient to express the resulting two port reflection coefficients σ_{22} and σ_{22} in terms of S_{11}, S_{12}, S_{13} and S_{14} as will be further pursued in the error analysis of Chapter 6. Furthermore, it follows from (3.2.2a) and (3.2.2b) that the larger the $\Delta\delta = \delta_{13} - \delta_{14}$, the smaller is the total transformation domain.

Chapter 4

3-db COUPLERS AS TUNING DEVICES

4.1 INTRODUCTION

At high power levels the type of tuner most commonly used is a "3-db short-slot" (coupler), which is a hybrid junction with short circuits in the two output arms as shown in (Fig.8). Earlier it was demonstrated that the E-H tuner is effective over a wide range of wave guide wave lengths, limited only by the effectiveness of the short circuit, losses and defects in symmetry and not by basic operating principle. The 3-db short-slot's tuning action is limited in frequency by its ability to maintain a 3-db power split, although it has the advantage of being usable at high power levels.

A general approach to a quantitative analysis of the operation of the '3-db short-slot' is possible by utilizing the special relationships for the scattering matrix of a four port, reciprocal lossless junction and the special properties associated with 3-db directional couplers. Expressions for the reflected wave at the input terminal will be developed. Again the range of the reflection coefficient that can be matched will be determined by deriving the range of the input reflection coefficient (impedance) that can be obtained with a match on the output terminal.

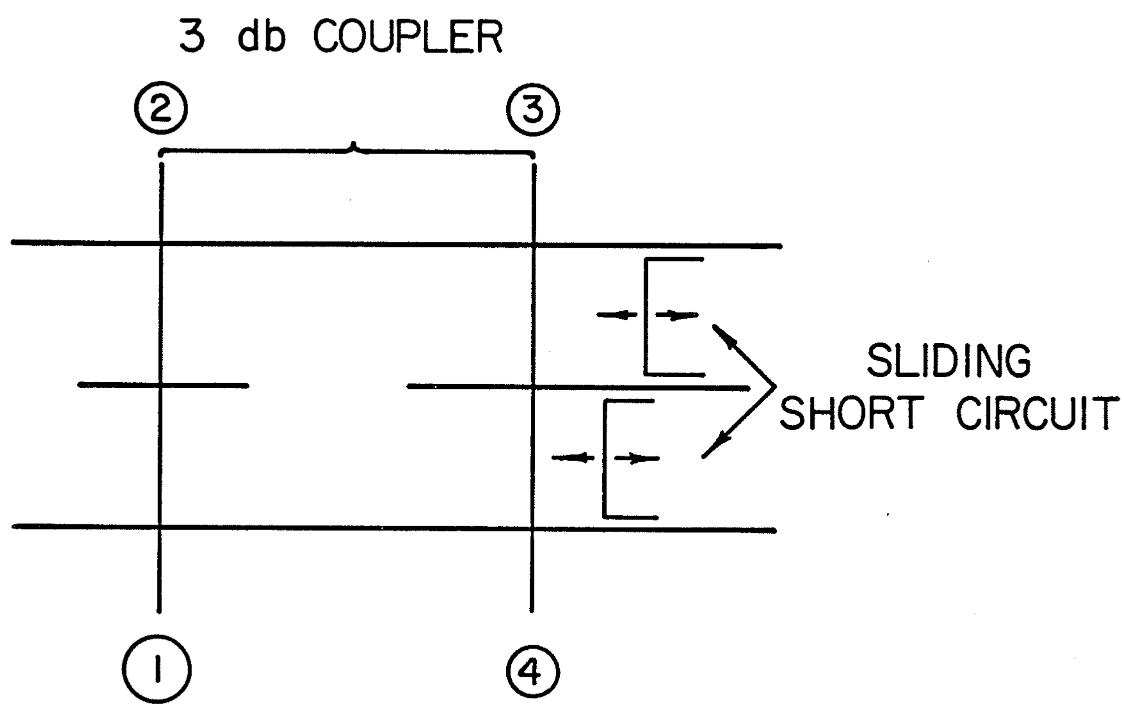

Fig. 8 Schematic of 3db "Short Slot" Tuner

4.2 PERFECTLY MATCHED 3-db COUPLER (IDEAL CASE)

Ref [11] gives the expression for the input reflection coefficient when it is possible to choose a symmetrical reference plane with respect to wave guide ports, such that the scattering matrix elements take on the following values,

$$S_{11} = S_{22} = S_{33} = S_{44} = 0 \qquad \text{(perfectly matched)}$$

$$S_{12} = S_{34} = 0 \qquad \text{(infinite directivity)}$$

and $S_{13} = \frac{1}{\sqrt{2}}$; $S_{14} = j\frac{1}{\sqrt{2}}$

and Γ_1 is given by,

$$\Gamma_1 = \sin\left(\frac{\phi_3 - \phi_4}{2}\right) \exp\left[j\left(\frac{\phi_3 + \phi_4}{2} + \pi/2\right)\right] \qquad (4.2.1)$$

where ϕ_3 is a linear measure of the distance between the short in arm 3 and the reference plane of port 3. ϕ_4 is a similar measure for the short in arm 4. The same reference has also analysed the influence of the coupler imperfection. However it was assumed that symmetry is still present and the junction is still matched and decoupled, but the coupling is not exactly 3-db. So,

$$S_{13} = \frac{1}{\sqrt{2}} \sqrt{1 + \Delta}$$

whence,

$$S_{14} = \frac{1}{\sqrt{2}} \sqrt{1 - \Delta}$$

where $\Delta \ll 1$ and thus the expression for the input reflection coefficient becomes

$$\Gamma_1 = \left[\Delta \cos\left(\frac{\psi_3 - \psi_4}{2}\right) + j \sin\left(\frac{\psi_3 - \psi_4}{2}\right)\right] \cdot \exp\left[j\left(\frac{\psi_3 + \psi_4}{2}\right)\right]$$

This shows that all values of the reflection coefficient may be generated except those having a magnitude less than Δ, or in other words, loads having a reflection coefficient magnitude less than Δ cannot be matched perfectly. The worst effect is that a perfectly matched load will not permit a reflection coefficient less than Δ at the input.

4.3 TRANSFORMATION LOCI OF MISMATCHED AND IMPERFECTLY COUPLED 3-db TUNERS

So far the case when all four ports are perfectly matched was discussed. This is a condition which is difficult to achieve in practice. In this section transformation properties are analysed when the terminals are not perfectly matched. However the assumption of symmetry and infinite directivity still holds true. Under these conditions the scattering matrix elements take on the following values,

$$S_{11} = S_{22} = S_{33} = S_{44} \neq 0 \qquad \text{(imperfect matching)}$$

$$S_{12} = S_{34} = 0 \qquad \text{(infinite directivity)}$$

$$\begin{aligned} S_{13} &= \frac{1}{\sqrt{2}}\sqrt{1+\Delta_1} \;; \qquad S_{14} = j\frac{1}{\sqrt{2}}\sqrt{1+\Delta_2} \\ S_{23} &= j\frac{1}{\sqrt{2}}\sqrt{1+\Delta_2} \;; \qquad S_{24} = \frac{1}{\sqrt{2}}\sqrt{1+\Delta_1} \end{aligned} \qquad (4.3.1)$$

where Δ_1 and Δ_2 are small perturbations in power split because of imperfect coupling. It is also assumed that

$\Delta_1 << 1 \cdot \Delta_2 << 1$

and $\Delta_1 \neq \Delta_2$

subjected to conditions (4.3.1), eqn.(2.2.6d) becomes

$$s_{22} = S_{22} + \frac{S_{23}^2}{(1/S_{55}-s_{33})} + \frac{S_{24}^2}{(1/S_{66}-S_{44})} \tag{4.3.2}$$

Eqn.(I-6b), gives S_{22} of the four port in terms of $S_{\mu 3}$ and $S_{\mu 4}$ [where $\mu = 1, 2, 3, 4$] and their conjugates:

$$S_{22} = \frac{1}{S_{13}^* S_{24}^* - S_{23}^* S_{14}^*} \left\{ S_{23}S_{14}^* S_{33}^* - (S_{13}^* S_{23} - S_{14}^* S_{24}) S_{34}^* - S_{13}^* S_{24} S_{44}^* \right\}$$

but, also because of symmetry and infinite directivity,

$$S_{13} = S_{24} \qquad \text{and} \qquad S_{14} = S_{23} \qquad \text{and} \qquad S_{34} = 0$$

so,

$$S_{22} = \frac{1}{S_{24}^{*2} - S_{23}^{*2}} \{ S_{33}^* |S_{23}|^2 - S_{44}^* |S_{24}|^2 \}$$

from eqn.(4.3.1),

$$S_{24}^{*2} = S_{24}^2 = \tfrac{1}{2}(1 + \Delta_1)$$

$$S_{23}^{*2} = -S_{23}^2 = -\tfrac{1}{2}(1 + \Delta_2)$$

so,

$$(S_{24}^{*2} - S_{23}^{*2}) = 1 + \tfrac{1}{2}(\Delta_1 + \Delta_2) = 1 + \Delta'$$

where Δ' is the average of the two perturbations Δ_1 and Δ_2 i.e.

$$\Delta' = \tfrac{1}{2}\ (\Delta_1 + \Delta_2)$$

substituting all these in the expression for the four port S_{22},

$$S_{22} = (S_{33}^* |S_{23}|^2 - S_{44}^* |S_{24}|^2)/(1+\Delta') \tag{4.3.3}$$

and thus equation (4.2) for equivalent s_{22} becomes

$$s_{22} = \frac{1}{1+\Delta'} \left[\frac{S_{23}^2(1+\Delta') - |S_{33}|^2 |S_{23}|^2 + S_{33}^*/S_{55} |S_{23}|^2}{(1/S_{55}-S_{33})} + \frac{S_{24}^2(1+\Delta') + |S_{44}|^2 |S_{24}|^2 - \frac{S_{44}^*}{S_{66}} |S_{24}|^2}{(1/S_{66}-S_{44})} \right] \tag{4.3.4}$$

From expression (4.3.1), it is found that

$$|S_{23}|^2 = -S_{23}^2 \qquad \text{and} \qquad |S_{24}|^2 = S_{24}^2$$

and thus

$$s_{22} = \frac{|S_{23}|^2}{1+\Delta'} \left\{\frac{S_{33}^*/S_{55}-|S_{33}|^2-(1+\Delta')}{(1/S_{55}-S_{33})}\right\} + \frac{|S_{24}|^2}{1+\Delta'} \left\{\frac{1+\Delta'+|S_{44}|^2-S_{44}^*/S_{66}}{(1/S_{66}-S_{44})}\right\} \tag{4.3.5}$$

Eqns (I-4b) and (I-4e)give, [after putting $S_{34} = 0$]

$$|S_{13}|^2 + |S_{23}|^2 + |S_{33}|^2 = 1$$

and $$|S_{14}|^2 + |S_{24}|^2 + |S_{44}|^2 = 1$$

Putting values of $|S_{13}|^2$, $|S_{23}|^2$, $|S_{14}|^2$ and $|S_{24}|^2$ into these two equations, it is found

$$|S_{33}|^2 = -\Delta'$$

$$|S_{44}|^2 = -\Delta'$$

which imposes another condition on Δ_1 and Δ_2 i.e.

$$\Delta_1 + \Delta_2 < 0$$

now

$$s_{22} = \frac{|S_{23}|^2}{1+\Delta'} \left\{ \frac{S_{33}^*/S_{55}-1}{1/S_{55}-S_{33}} \right\} - \frac{|S_{24}|^2}{1+\Delta'} \left\{ \frac{\frac{S_{44}^*}{S_{66}} - 1}{1/S_{66}-S_{44}} \right\} \tag{4.3.6a}$$

or

$$s_{22} = \tfrac{1}{2}\left(\frac{1+\Delta_2}{1+\Delta'}\right) \left[\frac{S_{33}^*/S_{55}-1}{1/S_{55}-S_{33}}\right] - \tfrac{1}{2}\left(\frac{1+\Delta_1}{1+\Delta'}\right)\left[\frac{S_{44}^*/S_{66}-1}{1/S_{66}-S_{44}}\right] \tag{4.3.6b}$$

according to eqn (2.2.1f), define

$$s_{55} = -\exp(-2\phi_3)$$

$$s_{66} = -\exp(-2j\phi_4)$$

where $\phi_3 = \beta\ell_3$ and $\phi_4 = \beta\ell_4$.

Here β is the imaginary part of the propagation constant i.e. $\beta = 2\pi/\lambda g$, λg being guide wave length.

writing; $S_{33} = |S_{33}|\exp(j\phi_{33})$

and $S_{44} = |S_{44}|\exp(j\phi_{44})$

the expression for s_{22} of eqn (4.3.6b) becomes,

$$s_{22} = \tfrac{1}{2}\left(\frac{1+\Delta_2}{1+\Delta'}\right)\left[\frac{1+|S_{33}|\exp j(2\phi_3-\phi_{33})}{1+|S_{33}|\exp -j(2\phi_3-\phi_{33})}\right]\exp(-2j\phi_3)$$
$$- \tfrac{1}{2}\left(\frac{1+\Delta_1}{1+\Delta'}\right)\left[\frac{1+|S_{44}|\exp j(2\phi_4-\phi_{44})}{1+|S_{44}|\exp -j(2\phi_4-\phi_{44})}\right]\exp(-2j\phi_4) \qquad (4.3.7)$$

For the convenience of further analysis, redefine the zero setting of the adjustable stubs $\ell_p = \ell_3$ and $\ell_s = \ell_4$ with respect to fixed reference planes of the H and E arms. So define,

$$\phi_3' = \phi_3 - \phi_{33}/2$$

$$\phi_4' = \phi_4 - \phi_{44}/2$$

Then eqn (4.3.7) becomes

$$s_{22} = \tfrac{1}{2}\left(\frac{1+\Delta_2}{1+\Delta'}\right)\left[\frac{1+|S_{33}|\exp(2j\phi_3')}{1+|S_{33}|\exp(-2j\phi_3')}\right]\exp(-2j\phi_3) \qquad (4.3.8)$$
$$- \tfrac{1}{2}\left(\frac{1+\Delta_1}{1+\Delta'}\right)\left[\frac{1+|S_{44}|\exp(2j\phi_4')}{1+|S_{44}|\exp(-2j\phi_4')}\right]\exp(-2j\phi_4)$$

now define,

$$\theta_3 = \tan^{-1}\left[\frac{|s_{33}|\sin 2\phi_3'}{1+|s_{33}|\cos 2\phi_3'}\right] \qquad (4.3.9a)$$

and

$$\theta_4 = \tan^{-1}\left[\frac{|s_{44}|\sin 2\phi_4'}{1+|s_{44}|\cos 2\phi_4'}\right] \qquad (4.3.9b)$$

then,

$$s_{22} = \tfrac{1}{2}\left(\frac{1+\Delta_2}{1+\Delta'}\right)\exp[2j(\theta_3-\phi_3)] - \tfrac{1}{2}\left(\frac{1+\Delta_1}{1+\Delta'}\right)\exp[2j(\theta_4-\phi_4)]$$

Let,

$$\psi_4(\phi_4 = \text{const},\ \phi_3 = \text{variable}) = 2(\theta_3-\phi_3)$$

$$\psi_3(\phi_3 = \text{const},\ \phi_4 = \text{variable}) = 2(\theta_4-\phi_4)$$

so that,

$$s_{22} = \tfrac{1}{2}\left(\frac{1+\Delta_2}{1+\Delta'}\right)\exp(j\psi_4) - \tfrac{1}{2}\left(\frac{1+\Delta_1}{1+\Delta'}\right)\exp(j\psi_3)$$

after replacing Δ_1 by $(2\Delta'-\Delta_2)$ and readjusting

$$\begin{aligned} s_{22} &= \tfrac{1}{2}\cdot\frac{1}{1+\Delta'}[\exp(j\psi_4)-\exp(j\psi_3)] \\ &\quad + \frac{\Delta_2}{2(1+\Delta')}[\exp(j\psi_4)+\exp(j\psi_3)] - \left[\frac{\Delta'}{1+\Delta'}\exp(j\psi_3)\right] \end{aligned} \qquad (4.3.10)$$

This can be rewritten as

$$s_{22} = \frac{1}{1+\Delta'}\left[(\Delta_2-\Delta')\cos\left(\frac{\psi_4-\psi_3}{2}\right)+j(1+\Delta')\sin\left(\frac{\psi_4-\psi_3}{2}\right)\right]\exp j\left(\frac{\psi_4+\psi_4}{2}\right)$$

when Δ' is replaced by $\left(\frac{\Delta_1+\Delta_2}{2}\right)$, this expression becomes

$$\Gamma_2^* = s_{22} = \left[\frac{\Delta''}{1+\Delta'}\cos\left(\frac{\psi_4-\psi_3}{2}\right)+j\ \sin\left(\frac{\psi_4-\psi_3}{2}\right)\right]\exp j\left(\frac{\psi_3+\psi_4}{2}\right) \qquad (4.3.11)$$

where $\Delta'' = \frac{\Delta_2-\Delta_1}{2}$

From eqn (4.3.11) variation of the magnitude of the s_{22} of the equivalent two port junction is found out to be

$$\frac{\Delta''}{1+\Delta'} \leq |s_{22}| \leq 1 \quad \text{(for a lossless junction)} \qquad (4.3.12)$$

Eqn (4.3.12) shows that loads having reflection coefficient magnitude less than $\frac{\Delta''}{1+\Delta'}$ can not be matched perfectly. Also, since the magnitude of s_{22} can not be less than $(\Delta''/1+\Delta')$, a perfectly matched load at the output will give rise to an input reflection coefficient of $(\Delta''/1+\Delta')$.

4.4 COMPARISON OF TRANSFORMATION DOMAIN FOR A MATCHED AND AN IMPERFECTLY MATCHED 3-db TUNER

In section 4.2 it was shown that for perfectly matched and imperfectly coupled cases the load reflection coefficient cannot be less than Δ. Whereas in the case of an imperfectly matched junction it cannot be less than $\Delta''/1+\Delta'$. The conditions imposed on Δ_1, Δ_2 are

$$\Delta_1 \neq \Delta_2$$

and $$\Delta_1 + \Delta_2 < 0$$

now if it is assumed that imperfection in power is 0.1 db i.e.

$$s_{13} = 3\text{-db} \pm 0.1 \text{ db}.$$

then $$|\Delta| = 0.023.$$

In the case of an imperfectly matched 3-db tuner, let

$$|\Delta_1| = 0.023 \qquad \text{(corresponding to } 3 \pm 0.1 \text{ db)}$$

and $$|\Delta_2| = 0.031 \qquad \text{(corresponding to } 3 \pm 0.12 \text{ db)}$$

Here there can be two cases:

Case (i) Δ_1 and Δ_2 both are negative

so, $$\Delta_1 + \Delta_2 < 0$$

now $$\Delta'' = 0.004$$

$$\Delta' = -0.027$$

and thus $$\left|\frac{\Delta''}{1+\Delta'}\right| = \left|\frac{0.004}{1-0.027}\right| = 0.00412$$

Case (ii) $$\Delta_1 = \text{positive} = +0.023$$

$$\Delta_2 = \text{negative} = -0.031$$

hence $$\Delta_2 + \Delta_1 < 0$$

now, $$\Delta'' = -0.027$$

and $\Delta' = -0.004$

therefore $\left|\frac{\Delta''}{1+\Delta'}\right| = \left|\frac{-0.027}{1-0.004}\right| = 0.0271$

This shows that the performance of an imperfectly matched 3-db tuner could be better than that of a perfectly matched 3-db tuner, provided the imperfection in power split (coupling) is such that, Δ_1 and Δ_2 both are negative. This is true only at one end of the band.

Chapter 5

MEASUREMENTS

5.1 PURPOSE OF MEASUREMENTS

Although the term "network parameters" is usually associated with lumped equivalent circuit representations, it will be taken here to refer also to the elements of any description which characterize the input-output behaviour of the structure, and in particular, matrix representations. The choice of the scattering matrix representation was influenced by the following considerations

(a) ultimate use of the structure; the network operates as a complex conjugated load matching device.

(b) type of information required directly, i.e. locus of the s_{22} of the equivalent two port, as the transformation angles ψ_3 and ψ_4 are varied.

5.2 GENERAL PROCEDURE

The structure to be measured is inserted into an experimental set-up (see Fig.4) with which the appropriate measurements can be taken, and the data is then analyzed to yield the desired properties of the experimental structure. The equipment must be capable of measuring the VSWR and location of the voltage minimum, from which the desired quantities can be calculated. The VSWR and location of the voltage minimum can be measured with a slotted line. The structure to be investigated is of transmission type. Of the transmission type structures the two port is of greatest importance since the measurement of the equivalent network parameters of multiport junctions can be reduced to the measurement of an appropriately selected series of two ports.

5.3 HIGH VSWR MEASUREMENTS

Self explanatory Fig.5 shows the complete measurement setup. Since the output is terminated in a sliding short, high VSWR i.e. expected in the slotted wave guide section. The detection of V_{min} for high VSWR values is difficult. In order to have sufficient accuracy of measurement, Owens' method [Owens, 1969] was followed. Owens proposed taking two d measurements in the vicinity of a null (see Fig.9). V_{ref} is selected to be some convenient level above the noise. For a particular k value of Probe-detector, measurements are made to find d_1 and d_2. It may be shown that;

$$\text{VSWR} = \sqrt{1 + \frac{k^2-1}{\sin^2(\frac{\pi d_2}{\lambda g})-k^2\sin(\frac{\pi d_1}{\lambda g})}} \tag{5.3.1}$$

For $k^2 = 2$ (square law detector), and when $\frac{\pi d_2}{\lambda g}$ and $\frac{\pi d_1}{\lambda g} << 1$, the above equation simplifies to

$$\text{VSWR} = 1 + \frac{\lambda^2 g}{\pi^2(d_2^2-d_1^2)} \tag{5.3.2}$$

The main advantage of the Owens method is that the measurements are concentrated around a standing wave minimum where the line voltage is low (low impedance) and the probe influence is then small.

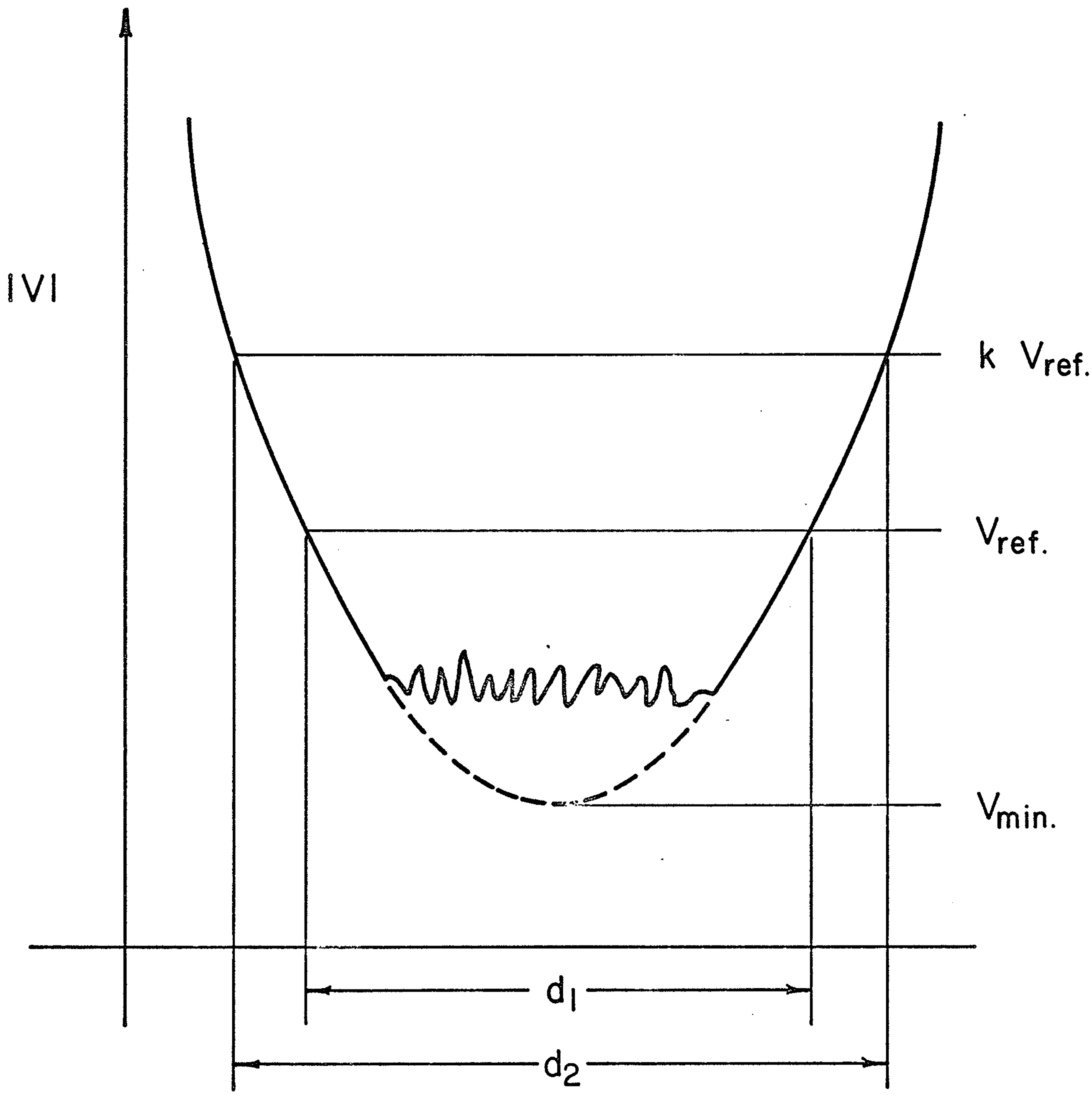

Fig. 9 Owens' Method of Measuring High VSWR

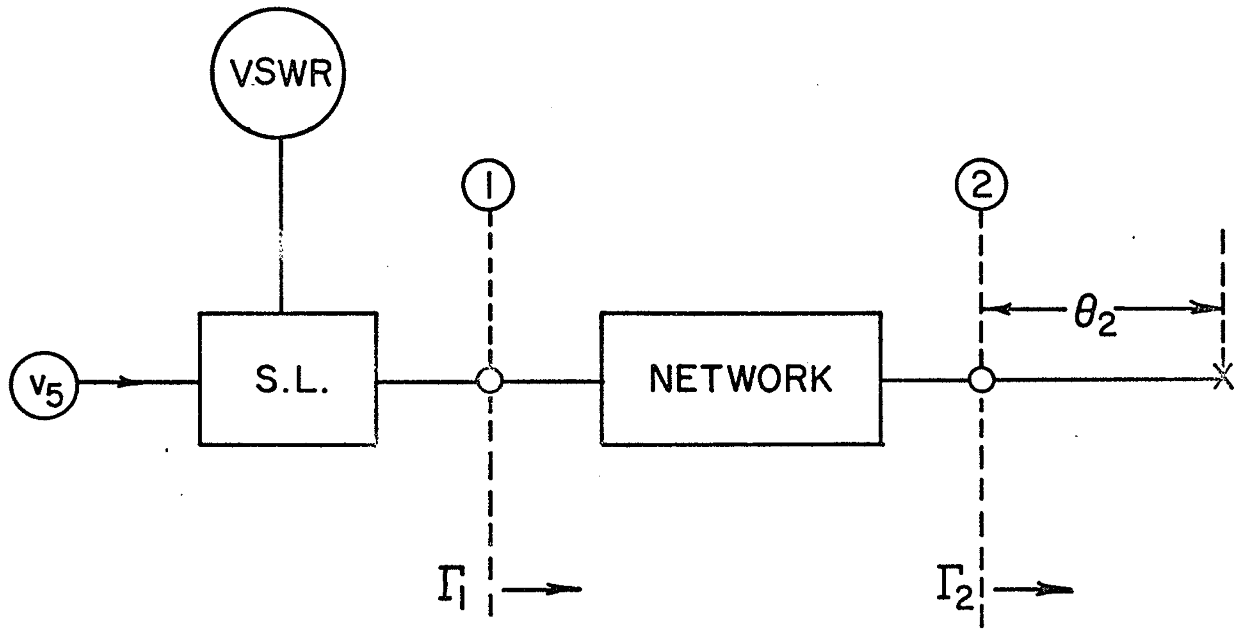

Fig. 10 Block Diagram for Owens' Method

5.4 DESCHAMPS METHOD (Measurement of scattering parameters of linear, reciprocal two ports)

Deschamps method involves a graphical solution of the equation

$$\Gamma_1 = s_{11} + \frac{s_{12}^2\Gamma_2}{1-s_{22}\Gamma_2} \qquad (5.4.1)$$

for the situation where Γ_2 is a pure reactive termination. Γ_2 is mapped (by measurement) into the Γ_1 plane. The usual measurement system follows: (see Fig.10).

$\Gamma_2 = -e^{2j\theta_2}$ is the unit circle in the reflection coefficient plane. In the experimental mapping, sample points of Γ_2 are taken so that θ_2 is some submultiple of $\lambda g/2$, i.e. $\Delta\theta_2 = \lambda g/16$, which gives 8 unique Γ_2 values. Γ_2 maps into a circle with points $\lambda g/\Delta$ apart being linked by diameters, i.e. d_2^1, d_2^5 are linked by a diameter (see Fig. 11a). d_2^1 corresponds to $\theta_2 = \pi/2$ and d_2^5 corresponds to $\theta_2 = 0$.

In mapping Γ_1 it is useful to recall the following conformal mapping theorems:

(a) A circular locus always maps into a circular locus, provided transformation is given by eqn. 5.4.1 .

(b) Angles between intersecting lines are preserved upon transformation.

An important point to be noted here is that the Γ_2 circle encloses all possible passive output terminations of the network and therefore the Γ_1 circle encloses all possible input impedance values.

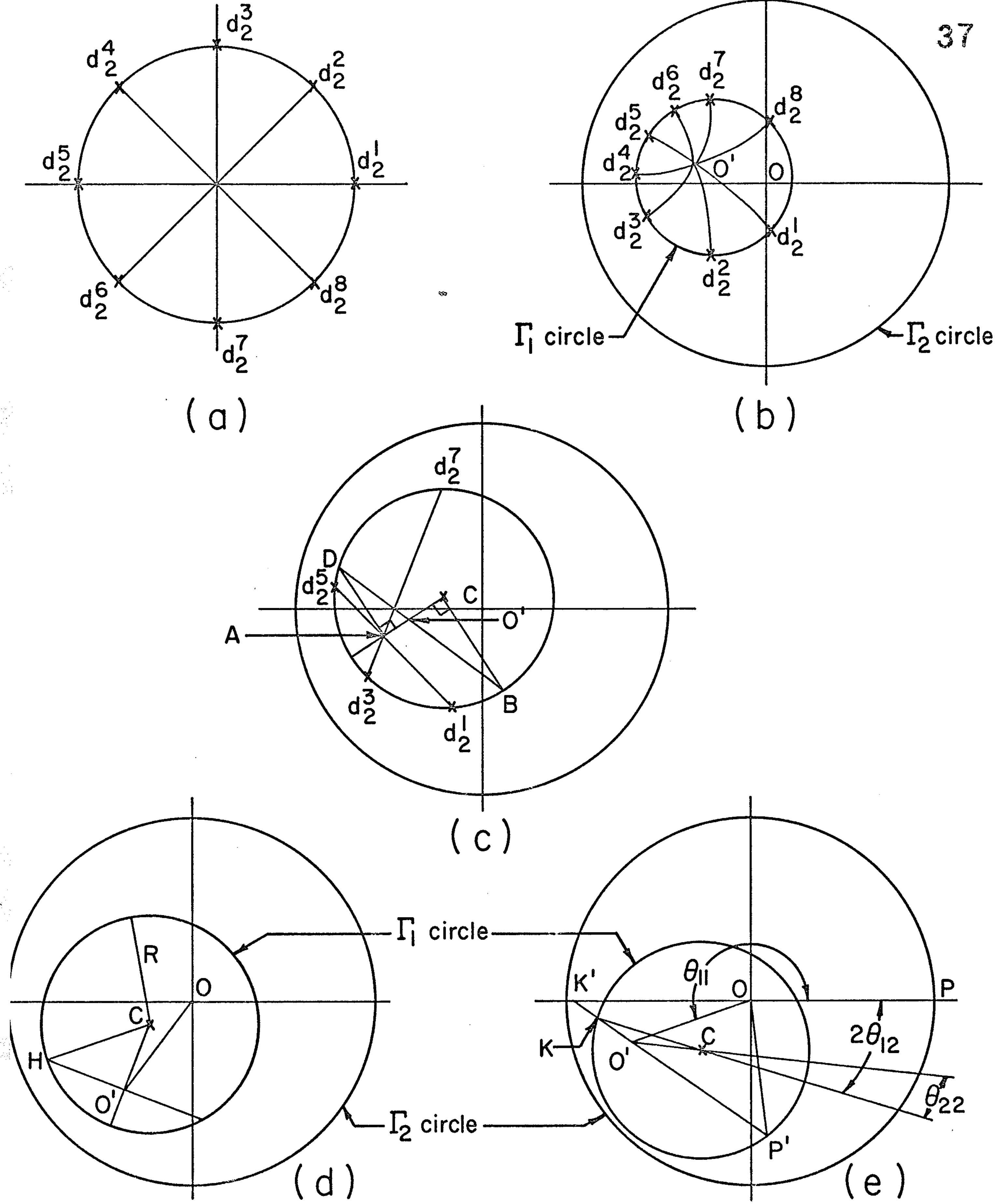

ig. 11 Deschamp' Method for Measuring Scattering Parameters

From theorem (a), Γ_1 maps into a circle for $\Gamma_2 = -e^{2j\theta_2}$ (see Fig. 11b). O' is called the iconocenter of the Γ_1 circle and corresponds to $\Gamma_2 = 0$, i.e. a matched load terminating the network.

The Graphical method used for locating the iconocenter follows: (see Fig.11c)

(a) Connect two "Γ_2 diameter-connected" sets of frequency points by straight lines in the Γ_1 plane; call the intersection A.

(b) Draw a radius from C through A and drop perpendiculars to the circle circumference from C and A ; call the two points so located B and D.

(c) Draw a straight line from B to D. The intersection with the radius from C is the iconocenter O'. Once the iconocenter and the center of the Γ_1 circle are determined the scattering coefficients are obtained by the following construction: (see Fig.11d)

$$|s_{11}| = OO' \quad , \quad |s_{22}| = CO'/R$$

$$|s_{12}| = \frac{O'H}{\sqrt{R}} \quad \text{or} \quad |s_{12}|^2 = R(1-|s_{22}|^2)$$

If the phase of the scattering coefficients referred to the specific mechanical reference planes is required, then Γ_1 must be known for $\Gamma_2 = 1 \cdot \Gamma_2 = 1$ for a short circuit located $\lambda g/2$ from the specified output reference plane. (see Fig.11e).

P corresponds to $\Gamma_2 = 1$, P' corresponds to Γ_1 for $\Gamma_2 = 1$

$\phi_{11} = \angle OP, OO'$, $\phi_{22} = \angle CO', CK$

and $\phi_{12} = \angle K'P, K'C$

In the practical measurement setup reference planes are determined as follows:

(a) Match terminate the output and locate a minimum on the input line. At this plane $s_{11} = -|s_{11}|$ and one has the input reference plane located.

(b) Terminate the output with a short circuit and obtain the Γ_1 circle. Locate the center and determine Γ_1 for $\Gamma_2 = 1$.

(c) Move the output short until $\Gamma_1 = OP'$. The output reference plane is $\lambda g/4$ away from the short.

5.5 EXPERIMENTAL RESULTS

The measurement of $|s_{22}|$ and ϕ_{22} can be accomplished in the following manner. The output port is terminated in a sliding short. A series of measurements of VSWR and shift in position of minimum from the input reference plane are made corresponding to the positions of the output short which gives $\Gamma\theta_2 = n\lambda g/16$ (n being an integer up to 8). This was repeated for different settings of shorts in E and H arms i.e. for different values of transformation angles ψ_3 and ψ_4. Measurement data for symmetrical E-H tuners show that if port 1 or 2 is matched and one of the tunable short-circuited plungers is held on a fixed position whereas the other stub is moved over one-half wave length and vice versa, circular transformation loci for the input impedance results at port 2 or 1, respectively. Compiled data is given in Table I, and the corresponding plot of the transformation loci is as shown in (Fig.12).

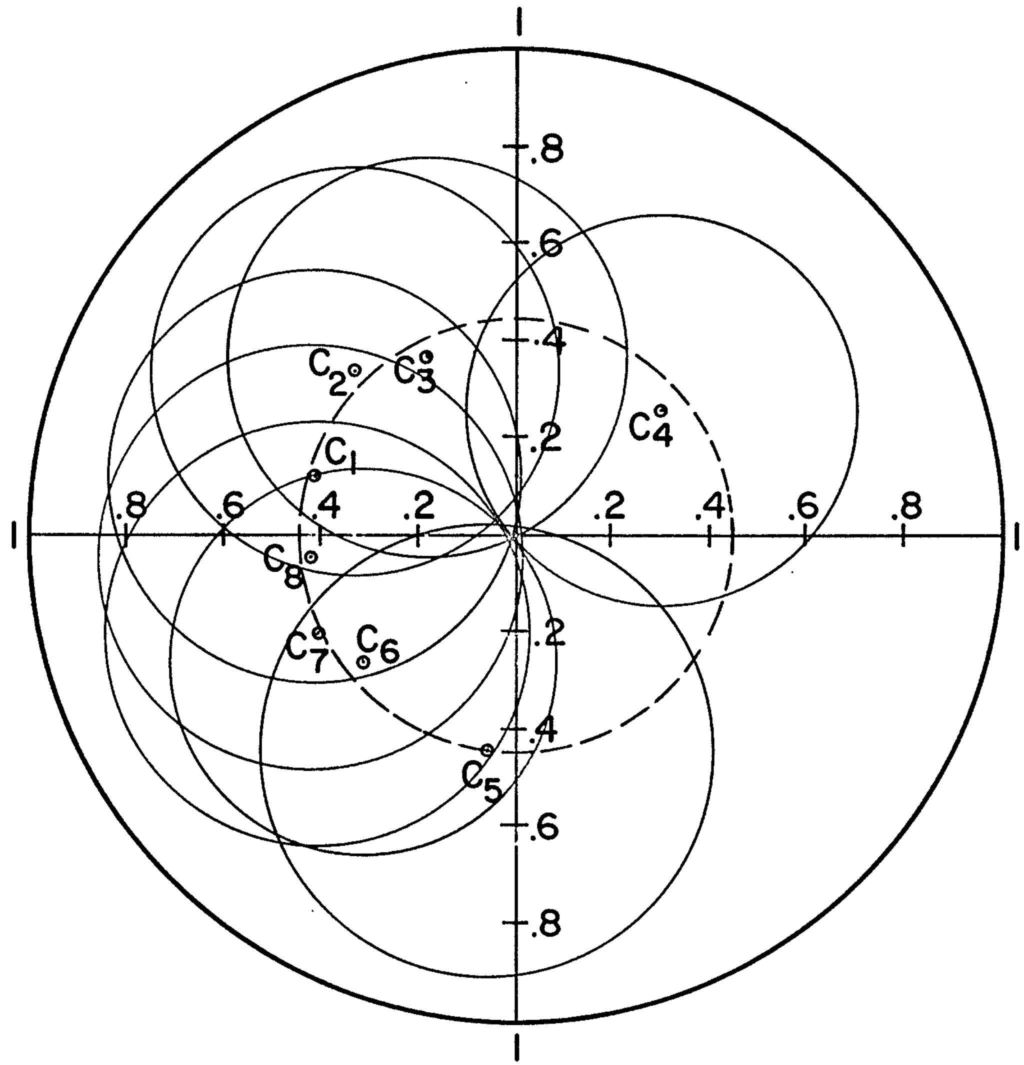

Fig. 12 Experimentally Determined Transformation Loci of E-H Tuner

TABLE - I

FREQUENCY = 9.474 GHz

$\lambda g/2$ (π elec. rad.) = 2.24 cms m

ϕ_3 = 0.0°			ϕ_3 = 20.0°			ϕ_3 = 40.0°			ϕ_3 = 60.0°		
ϕ_4 (in deg.)	magni-tude $\|S_{22}\|$	phase ϕ_{22} (deg.)	ϕ_4 (in deg.)	magni-tude $\|S_{22}\|$	phase ϕ_{22} (deg.)	ϕ_4 (in deg.)	magni-tude $\|S_{22}\|$	phase ϕ_{22} (deg.)	ϕ_4 (in deg.)	magni-tude $\|S_{22}\|$	phase ϕ_{22} (deg.)
0.0	0.475	71	0.0	0.627	102	0.0	0.760	79	0.0	-	-
20.0	0.351	93	20.0	0.454	90	20.0	0.616	73	20.0	0.955	13
40.0	0.126	87	40.0	0.305	82	40.0	0.521	68	40.0	0.880	25
60.0	0.078	114	60.0	0.1255	78.5	60.0	0.358	56	60.0	0.792	23
80.0	0.178	143	80.0	0.0474	107	80.0	0.1915	35	80.0	0.653	13
100.0	0.394	135	100.0	0.324	140	100.0	0.111	129	100.0	0.458	17
120.0	0.882	167	120.0	0.770	167	120.0	0.437	177	120.0	0.0382	155
140.0	-	-	140.0	-	-	140.0	-	-	140.0	0.624	80
160.0	0.712	118	160.0	0.773	104	160.0	0.824	108	160.0	1.00	0.0
180.0	0.416	90	180.0	0.558	92.5	180.0	0.702	74	180.0	-	-
ϕ_3 = 80°			ϕ_3 = 100°			ϕ_3 = 120°			ϕ_3 = 140°		
ϕ_4 (in deg.)	magni-tude $\|S_{22}\|$	phase ϕ_{22} (deg.)	ϕ_4 (in deg.)	magni-tude $\|S_{22}\|$	phase ϕ_{22} (deg.)	ϕ_4 (in deg.)	magni-tude $\|S_{22}\|$	phase ϕ_{22} (deg.)	ϕ_4 (in deg.)	magni-tude $\|S_{22}\|$	phase ϕ_{22} (deg.)
0.0	0.256	- 18	0.0	0.1315	+144	0.0	0.297	+130	0.0	0.406	+117
20.0	0.457	- 35	20.0	0.1094	- 68	20.0	0.0936	+135	20.0	0.198	+113
40.0	0.620	- 45	40.0	0.2565	- 71	40.0	0.073	+ 89	40.0	0.0312	+140
60.0	0.736	- 50	60.0	0.419	- 78	60.0	0.267	- 91	60.0	0.131	- 97
80.0	0.826	- 73	80.0	0.608	- 96	80.0	0.422	-101	80.0	0.318	-110
100.0	0.872	- 91	100.0	0.786	-120	100.0	0.666	-113	100.0	0.593	-132
120.0	-	-	120.0	-	-	120.0	1.000	-180	120.0	1.000	+180
140.0	0.497	-158	140.0	0.785	-171	140.0	0.851	+167	140.0	0.850	+162
160.0	0.0524	20	160.0	0.332	+151	160.0	0.497	+137	160.0	0.594	+130
180.0	0.330	- 26	180.0	0.354	+150	180.0	0.177	+110	180.0	0.319	+116

Chapter 6

APPLICATION OF ANALYTICAL TRANSFORMATION PROPERTIES AND ANALYSIS OF PARAMETERS REQUIRED TO BUILD AUTOMATED TUNING SYSTEMS

6.1 ANALYTIC-GEOMETRICAL INTERPRETATION OF THE TRANSFORMATION PROPERTIES

It must be shown that the load side reflection coefficient $\Gamma_2^* = s_{22}$ as given by (3.1.4) does indeed satisfy the experimental results described in the *Chapter 5* and illustrated in Figs.(6a) and (6b). Therefore in Appendix II, the load side reflection coefficient Γ_2^* is expressed in terms of either two intersecting circular or elliptical loci as derived in (II-3c) and (II-6c), respectively, and illustrated in Figs.13a, 13b and 13c. Comparing these resulting expressions with the experimental data and the derived expression for s_{22} as given in (3.1.4) in terms of the total transformation angles ψ_3 and ψ_4, it follows that (II-3c) does satisfy both (3.1.4) and the idealized experimental results, where

$$\Gamma = |\Gamma| \exp j\psi = \cos\left(\frac{\psi_3-\psi_4}{2}\right) \exp j\left(\frac{\psi_3+\psi_4}{2}\right) \qquad \text{(II-3c)}$$

Before the transformation properties of E-H tuners for particular design features are interpreted in relation with the phase constraints given in Appendix I, the general matching procedure for the total transformation angles ψ_3 and ψ_4 are analyzed and derived. In particular, two classes of matching problems must be solved.

(a) Given $\Gamma_{2_M}^* = s_{22}^M$ for which matching occurs, i.e. $\Gamma_1 = 0$, find the associated transformation angles, $\psi_3 = \psi_{3_M}$ and $\psi_4 = \psi_{4_M}$.

(b) Given ψ_{3_M} and ψ_{4_M} for which $\Gamma_1 = 0$, find $\Gamma_{2_M} = \overset{*}{s}_{22}$.

6.2 TRANSFORMATION PROPERTIES FOR THE LOSSLESS, SYMMETRICAL CASE

The explicit dependence of ψ_3 and ψ_4 on a given reflection coefficient Γ_2 is determined by (3.1.4) and (II-3c), where

$$\Gamma^*_{2_M} = \overset{M}{s}_{22} = +\cos\left(\frac{\psi_{3_M}-\psi_{4_M}}{2}\right)\exp j\left(\frac{\psi_{3_M}+\psi_{4_M}}{2}\right) \qquad (6.2.1a)$$

with ψ_{3_M} and ψ_{4_M} defining the total transformation angles for matching conditions, i.e. $\Gamma_1 = 0$.

If the complex loadside reflection coefficient Γ_{2_M} is given and characterized by its modulus $|\Gamma_M|$ and its phase ψ_{2_M}, it follows from (6.2.1a) that

$$\psi_{3_M} = -\psi_{2_M}(\pm)\ |\phi_{2_M}| \qquad (6.2.1b)$$

$$\psi_{4_M} = -\psi_{2_M}(\mp)\ |\phi_{2_M}| \qquad (6.2.1c)$$

where

$$|\phi_{2_M}| = |\text{arc}\cos(|\Gamma_{2_M}|)| \qquad (6.2.1d)$$

Reinspecting the generalized form of (3.1.4) and (II-3c), it is obvious that the total transformation angles ψ_{3_M} and ψ_{4_M} are not distinguishable and may be interchanged as is verified in (6.2.1b) and (6.2.1c) and shown in Fig.13b. This inherent degree of freedom is also evident from the definitions given in (II-4)and (II-5). Therefore, two pairs of solutions are obtained in addition to the

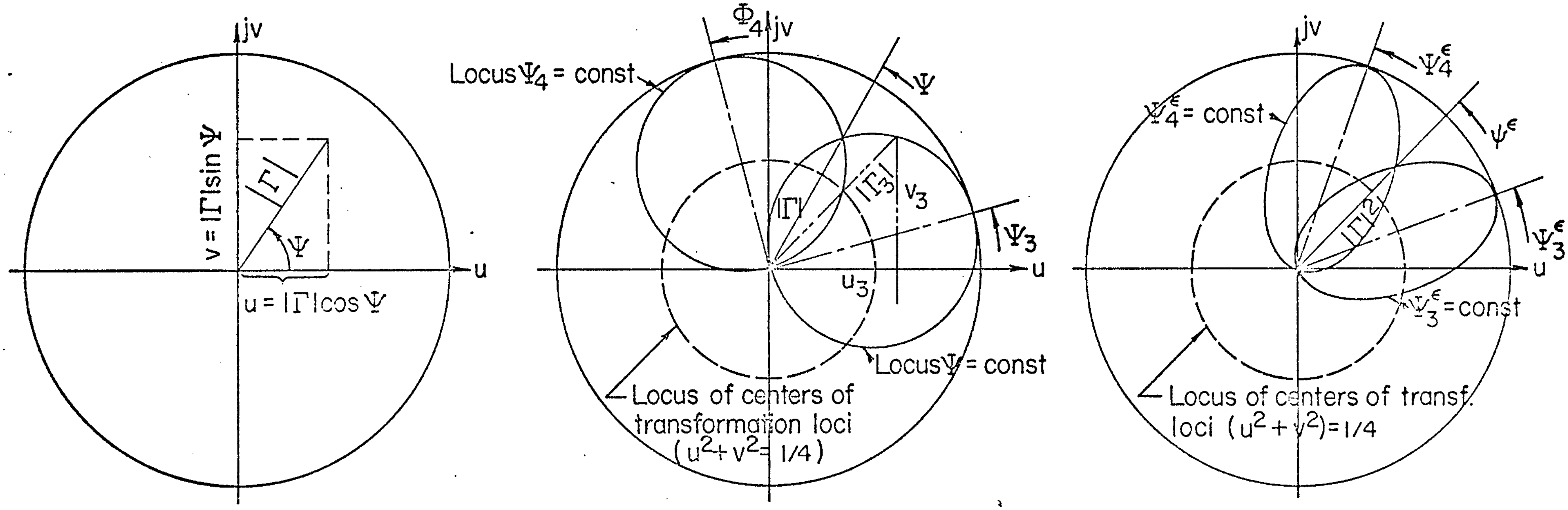

a. Complex Reflection Coefficient (Argand Plane)

b. Intersecting Circular Loci

c. Intersecting Elliptical Loci

Fig. 13 Analytical Interpretation of the Transformation Loci sets of periodic multiples.

Since $\phi 2_M = \text{arc}\cos(|\Gamma 2_M|)$ defines, for $0 \leq |\Gamma 2_M| \leq 1$, the equation of a circle, $C2_M$, in polar coordinates as defined in Fig.14a, it is possible to introduce a simple analytical procedure of determining $\psi 3_M$ and $\psi 4_M$.

6.3 GRAPHICAL PLOTTING PROCEDURE FOR THE DETERMINATION OF $\psi 3_M$ AND $\psi 4_M$, GIVEN $\Gamma 2_M$ (i.e. $|\Gamma 2_M|$ and $\psi 2_M$) (Figs. 14a and 14b)

Plot the $|\Gamma 2_M|$ circle, centered at the origin and having a radius of $|\Gamma 2_M|$, onto the polar Γ-plane. Draw the radius vector A making an angle of $-\psi 2_M$ with the real axis (0°). The resulting intersection with the $|\Gamma 2_M|$ circle defines $\overset{*}{\Gamma} 2_M = \overset{M}{s}_{22}$. The circle $|C\phi 2_M|$, defined as $|\phi 2_M| = |\text{arc}\cos(|\Gamma 2_M|)|$, is plotted such that its symmetry axis is the radius vector A. The intersection points P_3 and P_4 of circles $|C\phi 2_M|$ and $|\Gamma 2_M|$ then define the desired total transformation angles $\psi 3_M$ and $\psi 4_M$. Thus associated radius vectors B and C represent the symmetry axis of the circular transformation loci $\phi 3_M$ (ψ_3 = const, ψ_4 = adjustable) and $\phi 4_M$ (ψ_4 = const, ψ_3 = adjustable), whose intersection point defines $\overset{*}{\Gamma} 2_M = \overset{M}{s}_{22}$ according to equation (6.2.1a) and is shown in Fig.14b. It is evident that the total transformation angles are indistinguishable and do not, in general, represent the electrical transformation length ϕ_3 and ϕ_4 as defined in (3.1.3).

a. Polar Representation of
$\phi_{2M} = \arccos(|\Gamma_{2M}|)$

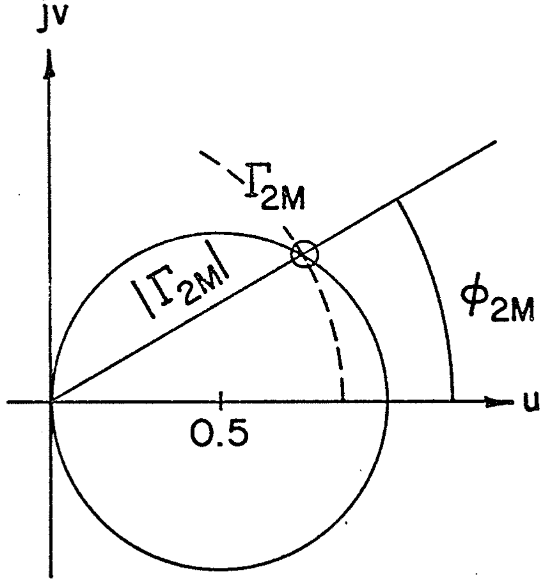

b. Graphical Evaluation

$\psi_{4M} = -\psi_{2M} (\mp) |\phi_{2M}|$

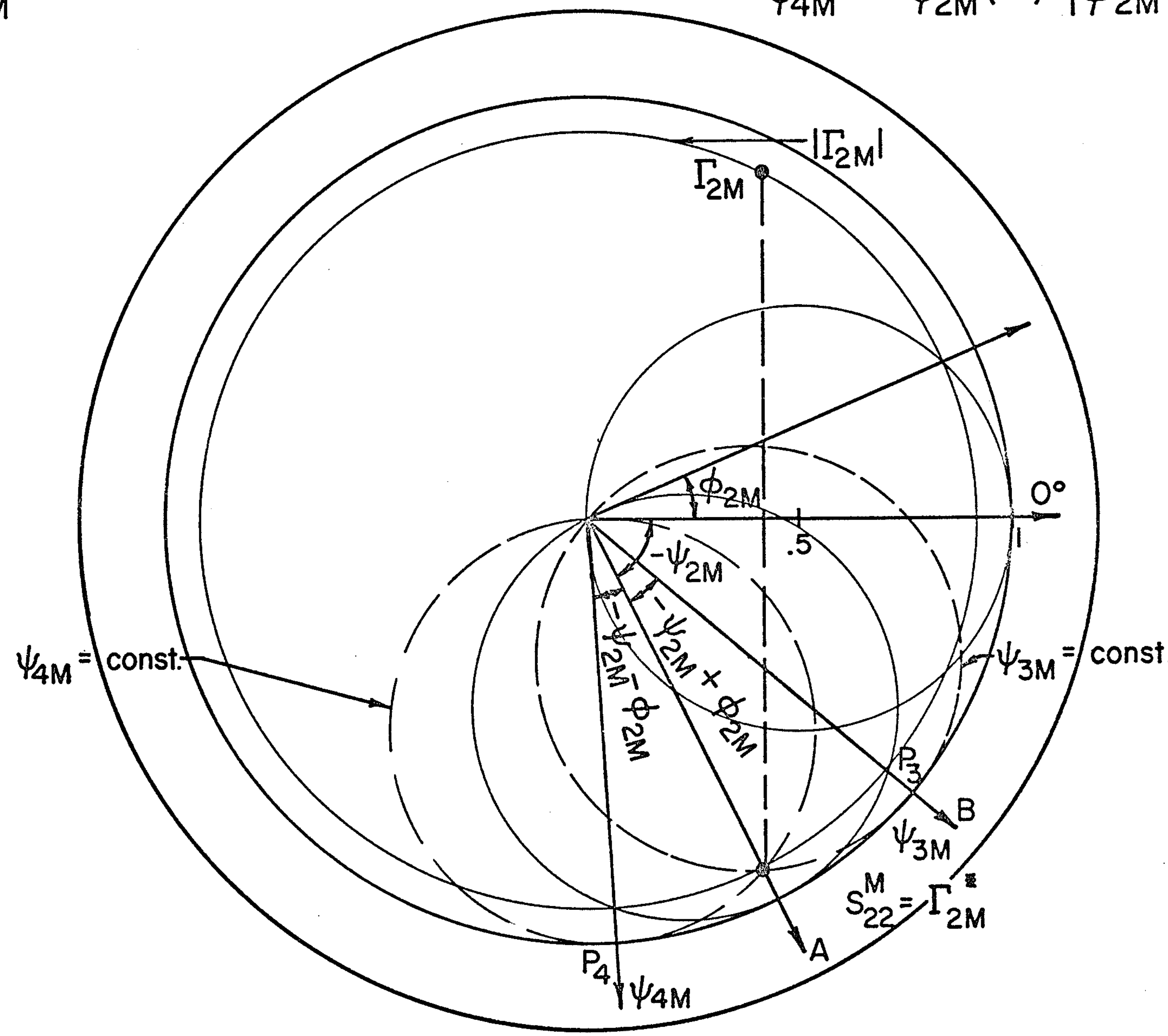

Fig. 14 Graphical Determination of the Transformation Angles

6.4 GRAPHICAL DETERMINATION OF $\Gamma_{2_M} = s_{22}^{M*}$, GIVEN ψ_{3_M} AND ψ_{4_M} (Fig. 14b)

If it is assumed that the generator side is match-isolated or means are provided to establish that $\Gamma_1 = 0$ and that the transformation properties of the employed E-H tuner are precisely established, then $\Gamma_{2_M} = s_{22}^{M*}$ is determined by definition of (6.2.1a) as

$$|\Gamma_{2_M}| = \cos\left(\frac{\psi_{3_M} - \psi_{4_M}}{2}\right) \qquad (6.4.1a)$$

$$\psi_{2_M} = -\left(\frac{\psi_{3_M} + \psi_{4_M}}{2}\right) \qquad (6.4.1b)$$

The analytical determination employs the inverse steps of the plotting procedure described in Section 6.3, is illustrated in Fig.14b, and therefore uniquely defined. It is to be noted that a unique solution for the determination of Γ_2 can always be obtained as verified by (6.4.1), although ψ_3 and ψ_4 are indistinguishable. However, in the case of this particular matching problem, the design of such an E-H tuner must be sought for which the dependence of ψ_3 on ϕ_4 and ψ_4 on ϕ_3 is most stable, i.e. linearly proportional.

6.5 ALTERATIONS OF THE TRANSFORMATION DOMAIN DUE TO LOSSES IN THE TRANSFORMATION STUBS

Since for all practical design reasons it may be assumed that the wave guide junction itself is lossless, the losses due to imperfect tunable shorts as well as those due to wear of the stub guide walls must be considered in the definition of s_{55} and s_{66}. The resulting internal reflection coefficient for this case may be defined with (2.2.1e) by

$$s_{55} = -\exp(-2\alpha_3)\cdot\exp(-2j\phi_3) \tag{6.5.1a}$$

$$s_{66} = -\exp(-2\alpha_4)\cdot\exp(-2\phi_4) \tag{6.5.1b}$$

To obtain a straightforward understanding of the resulting alterations, the effects on the idealized matched symmetrical E-H tuner and the magic T junction are considered, in which case (3.3c) becomes:

$$\overset{MT}{s_{22}} = -\tfrac{1}{2}\{\exp(-2\alpha_3)\cdot\exp(-2j\phi_3)+\exp(-2\alpha_4)\cdot\exp(-2j\phi_4)\}$$

$$= -\tfrac{1}{2}\{(\exp{-2\alpha_3}+\exp{-2\alpha_4})\cos(\phi_3-\phi_4)+j(\exp{-2\alpha_3}-\exp{-2\alpha_4})\cdot\sin$$

$$(\phi_3-\phi_4)\}\ \exp{+j(\phi_3+\phi_4)} \tag{6.5.1c}$$

From inspection of (6.5.1c), it follows that the transformation domain for $\alpha_3 \neq \alpha_4 \neq 0$ is reduced to

$$\tfrac{1}{2}\left|\exp{-2\alpha_3}-\exp{-2\alpha_4}\right| \leq \left|\overset{MT}{s_{22}}\right| \leq \tfrac{1}{2}\left|\exp{-2\alpha_3}+\exp{-2\alpha_4}\right|$$

and for this particular asymmetrically lossy case, no unique solution exists as is shown in Fig.15a. However, for the symmetrically lossy case, for which $\alpha_3 = \alpha_4 = \alpha > 0$, the solution is as illustrated in Fig.15b. In particular, it is noticed that perfect matching is no longer possible, $\alpha_3 \neq \alpha_4 \neq 0$, which leads to a rather important design requirement, namely that preferably all tuners are of identical properties to reduce unavoidable mismatch. Only if this requirement is satisfied, i.e. $\alpha_3 = \alpha_4$, may the transformation procedures derived in Section 6.2 be employed. Otherwise no unique solution is obtained as illustrated in Fig.15a.

6.6 ANALYSIS OF PARAMETERS REQUIRED TO BUILD AUTOMATED TUNING SYSTEMS

When the actual control circuit is designed, it is required to determine a readily measureable quantity which could be used to provide a control signal for automatically adjusting the position of shorts in E and H arms.

One well known technique for monitoring real and imaginary components of the reflection coefficient consists of sampling and detecting the r.f. signal at four points in the wave guide which are separated by 1/8th of the guide wavelength. When the outputs of alternate detectors are subtracted, two signals are obtained which are proportional to real and imaginary parts of the reflection coefficient, referred to the plane of the first detector. So in order to drive the shorts in the E and H arms to tuned positions, there should be an expression for transformation angles ψ_{3_M} and ψ_{4_M} in terms of available control signals. (here it is real and imaginary part of the load side reflection coefficient)

Rewriting the equation (3.1.4c)

$$\Gamma^*_{2_M} = s^M_{22} = \cos\left(\frac{\psi_{3_M}-\psi_{4_M}}{2}\right)\exp j\left(\frac{\psi_{3_M}+\psi_{4_M}}{2}\right)$$

or

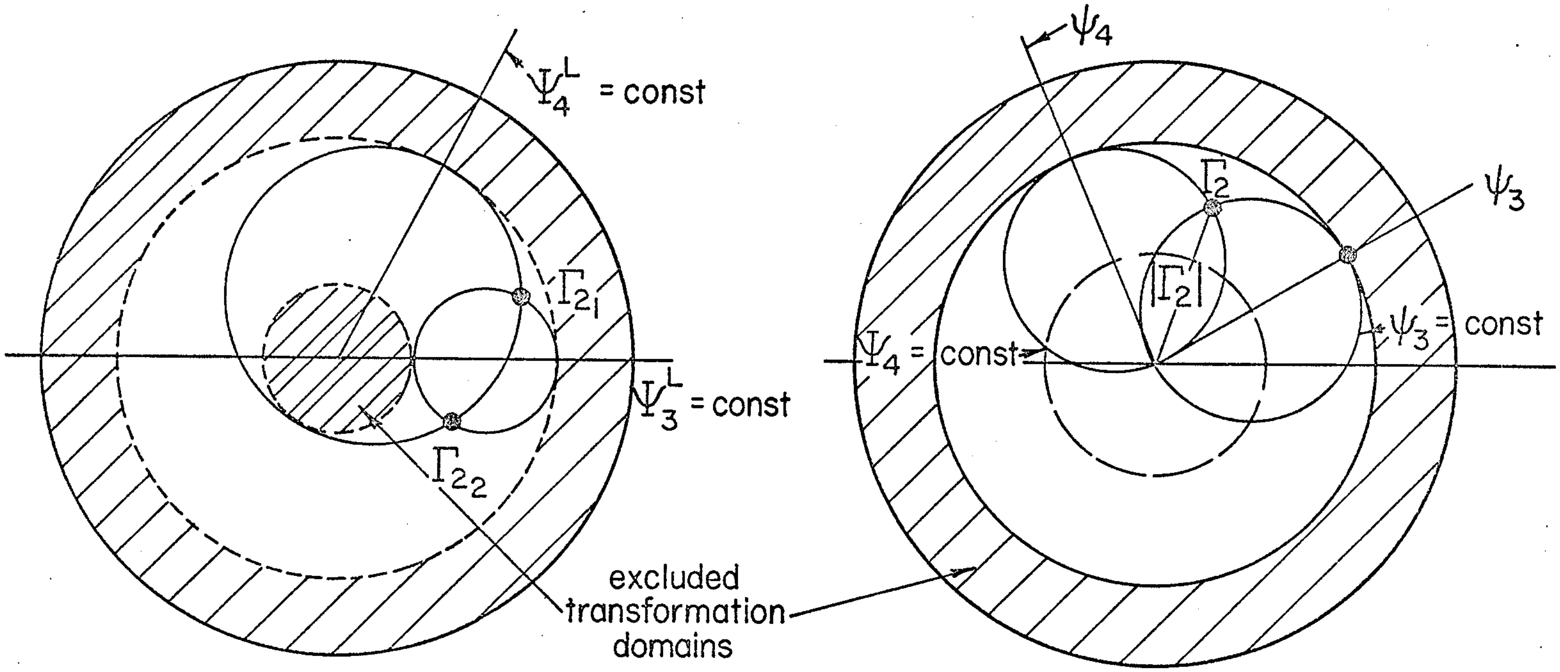

a. Asymmetrical Case

b. Symmetrical Case

Fig. 15 Transformation Properties for the Lossy Case

$$\Gamma_R - j\Gamma_i = \cos\left(\frac{\psi_{3_M}-\psi_{4_M}}{2}\right)\cos\left(\frac{\psi_{3_M}+\psi_{4_M}}{2}\right)$$

$$+ j\cos\left(\frac{\psi_{3_M}-\psi_{4_M}}{2}\right)\sin\left(\frac{\psi_{3_M}+\psi_{4_M}}{2}\right)$$

Here Γ_R is the real part of Γ_{2_M}, and Γ_i is the imaginary part of Γ_{2_M}. Using trigonometric identities and equating real and imaginary parts on both sides,

$$\cos\psi_{3_M} + \cos\psi_{4_M} = 2\Gamma_R \tag{6.6.1a}$$

$$\sin\psi_{3_M} + \sin\psi_{4_M} = -2\Gamma_i \tag{6.6.1b}$$

squaring both the equations

$$\cos^2\psi_{3_M}+\cos^2\psi_{4_M}+2\cos\psi_{3_M}\cos\psi_{4_M} = 4\Gamma_R^2 \tag{6.6.1c}$$

and

$$\sin^2\psi_{3_M}+\sin^2\psi_{4_M}+2\sin\psi_{3_M}\sin\psi_{4_M} = 4\Gamma_i^2 \tag{6.6.1d}$$

Adding eqn (6.6.1c) and (6.6.1d) and then subtracting eqn (6.6.1d) from eqn (6.6.1c) and readjusting the resulting equations,

$$\psi_{3_M} + \psi_{4_M} = \alpha_1$$

$$\psi_{3_M} - \psi_{4_M} = \alpha_2$$

where

$$\alpha_1 = \text{arc}\cos\left[\frac{4(\Gamma_R^2-\Gamma_i^2).}{4(\Gamma_R^2+\Gamma_i^2)-1}\right]$$

$$\alpha_2 = \text{arc}\cos[2(\Gamma_R^2+\Gamma_i^2)-1]$$

hence

$$\psi_{3_M} = \frac{\alpha_1+\alpha_2}{2}$$

and $$\psi_{4_M} = \frac{\alpha_1 - \alpha_2}{2}$$

These expressions will be used during description of the control circuit in *Chapter 7*.

Chapter 7

CONTROL CIRCUIT DESCRIPTION (E-H TUNER AS TUNING JUNCTION)

7.1 MONITORING THE LOAD REFLECTION COEFFICIENT AND GENERATING CONTROL SIGNALS (Fig. 16)

Since transformation angles ψ_{3_M} and ψ_{4_M} have been expressed in terms of real and imaginary parts of the load reflection coefficient, voltages equivalent to real and imaginary parts of the load side reflection coefficient are to be generated. These voltage levels in turn will be used as input for the circuits, which will generate voltage levels equivalent to transformation angles ψ_{3_M} and ψ_{4_M}.

The r.f. signal is sampled and detected at four points in the wave-guide which are separated by one-eighth of a guide wavelength (these four points are as near as possible to the load end). Outputs from these four detector probes 1, 2, 3, 4 are fed into preamplifiers I, II, III and IV respectively. The preamplifiers present a suitable input impedance and provide adjustable amplification to compensate for differences in the detectors and probes.

Outputs from pre-amps I and III are used as inputs in differential A, whose differential output gives the real part of the reflection coefficient existing on the waveguide (referred to the plane of the first detector). Similarly the outputs from pre-amps II and IV are fed into differential amplifier B and the imaginary part of the load reflection coefficient is generated.

The suggested circuit for the differential amplifier is a four-stage differential amplifier. [Ref: Texas Instruments Inc. "Transistor circuit design" McGraw Hill, N.Y., 1963, P.138]. An available circuit (which could be modified and improved upon) is designed for maximum open loop amplification of the differential signal. Series-shunt negative feedback provides high input impedance and low output impedance. The circuit responds to a differential signal of 25 microvolts superimposed on a common level that varies from 0 to 5.0V. The voltage gain is continuously variable from 100 to 500. The frequency response is flat within 1% from d.c. to 1000 Hz.

7.2 SQUARING AND FUNCTION GENERATING CIRCUITS

The expression for transformation angles ψ_{3_M} and ψ_{4_M} contains square terms of Γ_R the real part, and Γ_i the imaginary part of the load reflection coefficient. So the output from differential amplifiers A and B must be squared before they can be used in other function generating circuits. This is done by squaring circuits. Suggested references for the squaring circuits are given in the block diagram. However, the reference no. 3, "Square law output" seems to be better for the present application because of its flexibility, no critical or expensive components are used and it could be extended to large dynamic ranges if required. In this circuit a diode network and detector provide output proportional to the square of the input voltage. The input range of 40 db is split into two 20-db segments. Each stage saturates and gives constant output for voltages above operating range. For voltages below the operating range the stage is cut off and has zero output. The combination of two stages gives the desired square-law characteristic.

Function generators are in fact the heart of the whole system. Efficiency of the system depends very much on how accurately the function generators produce ψ_{3_M} and ψ_{4_M}, the transformation angles required for complex conjugate matching. Again references for the function generators are given on the block diagram. Without looking at the performance practically, it is difficult to suggest any particular circuit over other circuits. But in this particular case, the idea of "photo electric function generators" seems to have more potential than any other circuit.

An "open loop photo electric function generator" can generate any single valued function with an accuracy of better than one percent. Functions of a function can be produced with slight operating modification. Many of the problems common to closed-loop operation have been eliminated.

Function generators are followed by averaging circuits whose outputs give voltage levels proportional to the values of the transformation angles ψ_{3_M} and ψ_{4_M} required to match the load reflection coefficient

Preamplifier I, II, III, IV

Present a suitable input impedance and provide adjustable amplification to compensate for differences in the detectors & probes.

Four Stage Differential Amplifier

Texas Instruments Inc. "Transistor Circuit Design", McGraw Hill, N.Y. 1963, p.138.

Function Generator

1. Electronics 33 No.13, p.75-76
2. Photoelectric Function Generator, Electronics 32 No.2, p.52-55.(1959)

Squaring Circuit

1. EEE 11 No.7 p.6-7
2. Audio FET Squaring Circuit, "Field Effect Transistors", McGraw Hill N.Y. 1965, p.83.
3. Square Law output, Electronics 39 No.18, p.95-97.(1966)

Servo Comparator Circuit

1. Chopper Transistor Simulate SPDT Switch, Electronics 37 No.22, P.75-76. (1964)

Motor Control Circuits

1. Two-Source Control, Electronics 33 No.41, p.76. (1960)
2. Triac-Diac Reversing Servo Control: varies speed and direction of 5 amp reversible series a.c. motor in accordance with d.c. control signal. Polarity of control signal determines direction of rotation.

   Control Engineering 11 p.75-76. (1964)

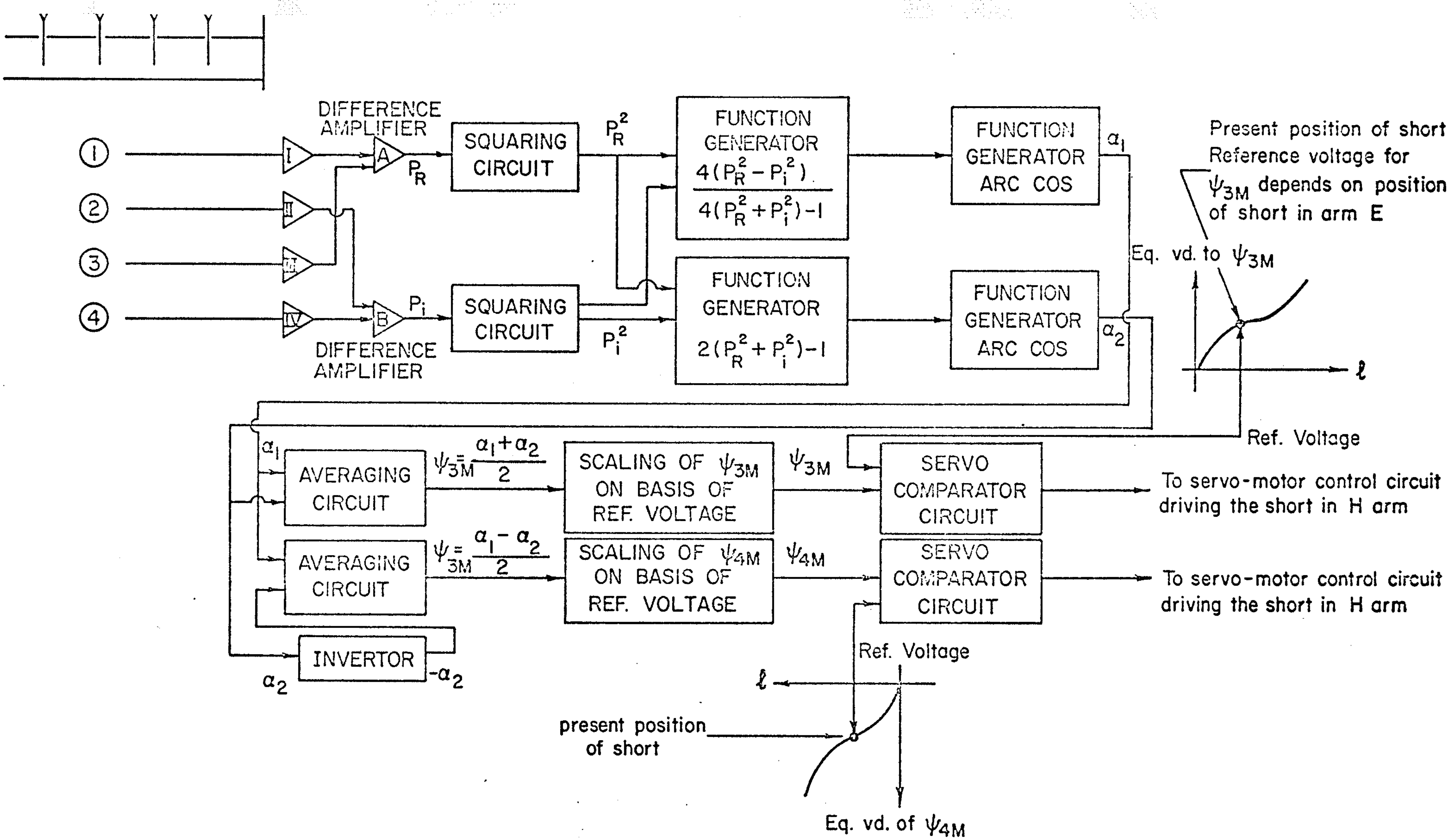

Fig. 16 BLOCK DIAGRAM OF PROPOSED CONTROL CIRCUIT

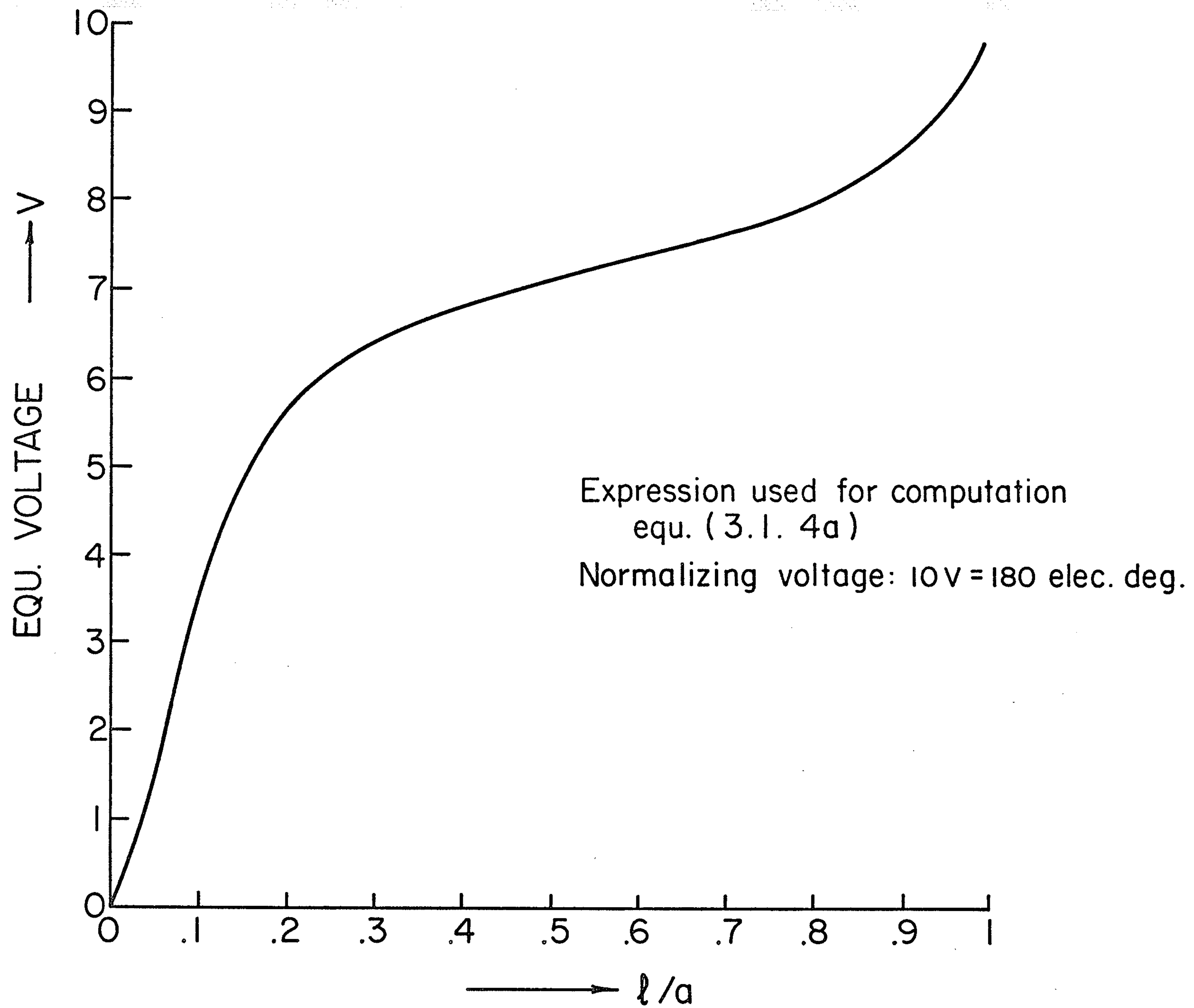

Fig. 17 Variation of Transformation Angle (Eq. Voltage) with Positioning of Short Circuiting Stub.

existing in the wave guide. Averaging circuits may be "differential amplifiers" preceeded by an inverter in one.

7.3 REFERENCE LEVEL

Without the information about the present position of the shorts in the E and H arms, it is not possible to operate the servo-motor, and bring the shorts to the tuned position. So a reference level is used and this reference level is controlled by the shorts in the E and H arms. This reference level is a voltage level which is equivalent to a transformation angle ψ_3 or ψ_4 corresponding to the original position of the shorts. A study of the variation of the transformation angle with the position of the short (in wavelength) gives the curve of Fig. 17. Again this voltage profile could be generated by a function generator. The input to this circuit could be controlled mechanically by the position of the tuning shorts. Thus the reference level gives complete information about the current position of the shorts. This level is compared with the level generated by the circuits whose input is controlled by the load side reflection coefficient (i.e. levels corresponding to ψ_{3_M} and ψ_{4_M}, the transformation angles required for matching the load to the input). The difference gives a measure of the distance, as well as the direction in which the shorts are required to be moved by the servo-motor.

7.4 SERVO COMPARATOR CIRCUIT

In this circuit, the generated control signal is compared with the reference voltage and thus a control signal for the servo-motor is generated. The suggested circuit for this purpose is a "Chopper transistors simulated SPDT switch" whose reference is given on the block diagram. This circuit controls up to 50 volts with an absolute error between reference and control voltage of less than two millivolts.

The circuit operates like a simple mechanical comparator system. The comparator chopper stage, driven by the oscillator, senses the difference between the reference voltage and the output signal of the system, but draws very little current from the reference.

7.5 MOTOR CONTROL CIRCUIT

Many kinds of motor control circuits are available. Specific advantages or disadvantages of a particular circuit could be understood only after practical study of the circuit under the condition which will prevail in practice. However a relatively simple, efficient and reliable circuit is "triac-diac reversing servo control", whose reference is given on the block diagram. This circuit uses a component called "triac" for a.c. power switching. This is a gate-controlled semiconductor switch which reduces the number of components required for a.c. power control and needs no protection from voltage transients.

This suggested circuit is a reversing drive servo-control circuit that varies the speed and direction of a series motor according to a d.c. control signal (which will be the output from the servo-comparator circuit in this case). The polarity of the control voltage determines the direction of motor rotation, and there is a gain pot that adjusts the slope of the speed versus the control voltage curve.

Chapter 8

SUMMARY AND CONCLUSIONS

An analytical closed form solution of the impedance transformation loci of various microwave junctions was derived. This solution was used to find out the transformation domain of the lossless, reciprocal 'hybrid T-junctions' as well as '3-db couplers'. These transformation domains allow one to determine the restrictions on the transformation properties of 'hybrid T-junctions' and "3-db couplers", used for matching purposes.

It can be concluded that for a given ideal, symmetrical hybrid T-junction (or '3 db-coupler') an arbitrary load side reflection coefficient Γ_2 for which $|\Gamma|<1$ can be transformed in all cases into $\Gamma_1 = 0$. In applying the E-H tuner as an imittance transformer, the H(3) and E(4) arms are terminated in tunable short-circuited plungers and by proper choice of the equivalent transformation lengths ℓ_3 and ℓ_4 from central symmetry planes, it is possible to transform the load dependent reflection coefficient Γ_2 (plane 2) into the input reflection coefficient $\Gamma_1 = 0$ (plane 1).

Measurement data compiled in *Chapter 5* for symmetrical E-H tuners show that if port 1 or 2 is matched and one of the tunable short-circuited plungers is held on fixed position whereas the other stub is moved over one-half wavelength and vice-versa, circular transformation loci for the input impedance results at the port 2 or 1 respectively. In particular it was found that for lossless case the entire passive region of the impedance plane can be transformed if the E and H arms are decoupled and not entirely mismatched. Slight asymmetrical phase shift in the transformation coefficients σ_{13}, σ_{23}, δ_{14} and σ_{24} of the E-H tuner results in coupling of the transformation arms. Furthermore, it follows from (3.2.2a) and (3.2.2b) that the larger the $\Delta\delta = \delta_{13} - \delta_{14}$, the smaller is the total transformation domain.

For an imperfectly coupled 3-db tuner eqn. 4.3.12 shows that loads having reflection coefficient magnitude less than $(\Delta''/1 + \Delta')$ can not be matched perfectly. Also, since the magnitude of s_{22} can not be smaller than $(\Delta''/1 + \Delta')$, a perfectly matched load at the output will give rise to an input reflection coefficient of $(\Delta''/1 + \Delta')$. It was also shown that the performance of an imperfectly matched 3-db tuner could be better than that of a perfectly matched 3-db tuner, provided the imperfection in power split (coupling) is such that, Δ_1 and Δ_2 both are negative.

In *Chapter 7* an electronic circuit is suggested with the help of the analytical transformation properties of E-H tuner, deduced in *Chapter 6*. A four probe sensor is used to provide control information and display the system match achieved by the tuner. Hybrid T-junction is to be employed in future as an automated, controllable impedance transformer in a measurement procedure based on the principle of complex conjugated impedance matching. One typical example of complex conjugated impedance matching is the measurement of the input impedance of non-linear, active microwave devices built into a rectangular waveguide supporting the dominant TE_{10} mode. Specifically this technique will be very helpful in the case for which the amplitude of the modulation signal must be held extremely small due to the non-linear behaviour of the active device (e.g. tunnel diode). Therefore, standard technique of employing slotted line measurement procedures must be excluded, since the resolution could be insufficient to obtain accurate measurement data.

The automated tuning device of *Chapter 7* would have great application in many microwave circuits. Because, although many systems maintain proper tuning for extended periods of time during operation, operator adjustment of the tuner is often required during start up procedures and is occasionally necessary during operation. When the system is detuned, full power transfer to the load is not achieved and efficiency of the circuit goes down. Consequently for most consistent results and operational convenience it is desirable to automate the adjustments of the system tuning mechanism.

REFERENCES

1. Altschuler, H.M., "The measurement of arbitrary linear microwave two-ports". The Institute of Electrical Engineers, Paper No. 3859E (May, 1962) pp.704-712 [Paper was presented at the Conference on Microwave Measurement Techniques, September 6,1961]

2. Belevitch, V., "Elementary applications of the scattering formalism in network design". IRE Transaction on Circuit Theory, 3 (June, 1956), pp.97-104.

3. Belevitch, V., "Four dimensional transformations of 4-pole matrices with applications to the synthesis of reactance 4-poles". IRE Transactions on Circuit Theory, 3 (June, 1956), pp.105-111.

4. Boerner, W.M., "Impedanznessung im S-band bei sehr kleinen Amplituden". Diploma Thesis, Technical Univ. Munich, Germany, 1963.

5. Brand, H., "Der Doppel-T-Anpassungstransformator". A.E.Ü. Band 18 [1964], Heft 3, pp.204-210.

6. Carlin, H.J., "The scattering matrix in network theory", IRE Transactions on Circuit Theory, 3 (June, 1956), pp.86-96.

7. Kahn, W.K., "Scattering equivalent circuits for common symmetrical junctions". IRE Transactions on Circuit Theory, 3 (June, 1956), pp.121-127.

8. Oono, Y., "Application of scattering matrices to the synthesis of n ports", IRE Transactions on Circuit Theory, 3 (June, 1956), pp.111-120.

9. Owens, R.P., "Technique for the measurement of VSWR at low power levels", Proc. IEE, 116, (June, 1969).

10. Stösser, W., "Das Magische T", Frequenz Bd. 14 (January, 1960) No.1, pp.17-19.

11. Sucher, M., and Fox, J., "Handbook of Microwave Measurements". Volume III, Chapter XXVI, pp.1133-1145. John Wiley & Sons. Inc. (1963) N.Y., London.

REFERENCES FOR SUGGESTED CIRCUITS

12. "Transistor Circuit Design". Texas Instruments Inc. McGraw Hill, N.Y. 1963, pp.138.

13. "Function Generator". Electronics 33, No.13, pp.75-76.

14. "Photoelectric Function Generator". Electronics 32, No.2, pp. 52-55 (1959).

15. "Squaring Circuit". EEE 11, No.7, pp.6-7.

16. "Audio FET Squaring Circuit". Field effect transistors. McGraw Hill, N.Y. 1965. pp.83.

17. "Square law output". Electronics 39, No.18, pp.95-97. (1966).

18. "Chopper Transistor Simulate SPDT Switch". Electronics 37, No. 22, pp.75-76. (1964).

19. "Two-Source Motor Control Circuits". Electronics 33, No.41, pp.76. (1960).

20. "Triac-Diac Reversing Servo Control". Control Engineering 11, pp.75-76. (1964).

RECOMMENDATION

The suggested tuned microwave circuit will offer a convenient means to efficiently couple microwave energy to widely varying loads. A typical example is microwave power transfer in a radar system, where the radiating or receiving antenna offers a varying impedance to the circuits. Another example of variable load microwave power application of the above circuit is in microwave heating. In microwave heating the suggested circuit could most efficiently transfer microwave energy to continuous thin web and filamentary types of material. This will not only be economic but also offer consistent product quality and operational convenience.

APPENDIX I

UNITARITY IDENTITIES

It is assumed that the hybrid junction is lossless and reciprocal but not a priori symmetrical, therefore the submatrices of $[S_H]$ must satisfy the following unitarity identities according to (2.2.2b)

$$[Q]^*[Q] + [T]^*[T]^T = [E] \tag{I-1a}$$

$$[Q]^*[T] + [T]^*[R] = [0] \tag{I-2a}$$

$$[T]^{*T}[Q] + [R]^*[T]^T = [0] \tag{I-3a}$$

$$[T]^{*T}[T] + [R]^*[R] = [E] \tag{I-4a}$$

where [E] and [0] represent the identity and null matrices, respectively, and the submatrices [Q], [T] and [R] are defined in (2.2.3c).

Evaluating the submatrix identities, yields

$$|s_{11}|^2 + |s_{12}|^2 + |s_{13}|^2 + |s_{14}|^2 = 1 \tag{I-1b}$$

$$\overset{*}{s}_{11}s_{12} + \overset{*}{s}_{12}s_{22} + \overset{*}{s}_{13}s_{23} + \overset{*}{s}_{14}s_{24} = 0 \tag{I-1c}$$

$$\overset{*}{s}_{12}s_{11} + \overset{*}{s}_{22}s_{12} + \overset{*}{s}_{23}s_{13} + \overset{*}{s}_{24}s_{14} = 0 \tag{I-1d}$$

$$|s_{12}|^2 + |s_{22}|^2 + |s_{23}|^2 + |s_{24}|^2 = 1 \tag{I-1e}$$

$$\overset{*}{s}_{11}s_{13} + \overset{*}{s}_{12}s_{23} + \overset{*}{s}_{13}s_{33} + \overset{*}{s}_{14}s_{34} = 0 \tag{I-2b}$$

$$\overset{*}{s}_{11}s_{14} + \overset{*}{s}_{12}s_{24} + \overset{*}{s}_{13}s_{34} + \overset{*}{s}_{14}s_{44} = 0 \tag{I-2c}$$

$$\overset{*}{s}_{12}s_{13} + \overset{*}{s}_{22}s_{23} + \overset{*}{s}_{23}s_{33} + \overset{*}{s}_{24}s_{34} = 0 \tag{I-2d}$$

$$\overset{*}{s}_{12}s_{14} + \overset{*}{s}_{22}s_{24} + \overset{*}{s}_{23}s_{34} + \overset{*}{s}_{24}s_{44} = 0 \tag{I-2e}$$

Since (I-3a) represents the complex conjugated transposition of (I-2a), no further useful identities are obtained

$$|s_{13}|^2 + |s_{23}|^2 + |s_{33}|^2 + |s_{34}|^2 = 1 \qquad \text{(I-4b)}$$

$$s_{13}^* s_{14} + s_{23}^* s_{24} + s_{33}^* s_{34} + s_{34}^* s_{44} = 0 \qquad \text{(I-4c)}$$

$$s_{14}^* s_{13} + s_{24}^* s_{23} + s_{34}^* s_{33} + s_{44}^* s_{34} = 0 \qquad \text{(I-4d)}$$

$$|s_{14}|^2 + |s_{24}|^2 + |s_{34}|^2 + |s_{44}|^2 = 1 \qquad \text{(I-4e)}$$

These identities are employed to derive the necessary and sufficient set of expressions enabling straightforward symmetry reduction, where from (I-1b) and (I-1e):

$$(|s_{11}|^2 - |s_{22}|^2) = (|s_{23}|^2 - |s_{13}|^2) + (|s_{24}|^2 - |s_{14}|^2) \qquad \text{(I-5a)}$$

(I-1c) and (I-1d)

$$s_{12} = \frac{-(s_{13}^* s_{23} + s_{14}^* s_{24}) s_{11} + (s_{13} s_{23}^* + s_{14} s_{24}^*) s_{22}}{(|s_{11}|^2 - |s_{22}|^2)} \qquad \text{(I-5b)}$$

(I-4b) and (I-4e):

$$(|s_{33}|^2 - |s_{44}|^2) = (|s_{14}|^2 + |s_{24}|^2) - (|s_{13}|^2 + |s_{23}|^2) \qquad \text{(I-5c)}$$

(I-4c) and (I-4d):

$$s_{34} = \frac{-(s_{13}^* s_{14} + s_{23}^* s_{24}) s_{33} + (s_{13} s_{14}^* + s_{23} s_{24}^*) s_{44}}{(|s_{33}|^2 - |s_{44}|^2)} \qquad \text{(I-5d)}$$

In addition, further explicit expressions for s_{11}, s_{12} and s_{22} in terms of $s_{\mu 3}$ and $s_{\mu 4}$ ($\mu = 1, 2, 3, 4$) and for s_{33}, s_{34} and s_{44} in terms of $s_{1\nu}$ and $s_{2\nu}$ ($\nu = 1, 2, 3, 4$) are required to simplify the expressions of the equivalent two-port scattering matrix parameters $s_{\mu\nu}$ given in (3.1.2), where from (I-2b) and (I-2c):

$$s_{11}=\frac{1}{(s_{13}^{*}s_{24}^{*}-s_{23}^{*}s_{14}^{*})}\{s_{13}s_{24}^{*}s_{33}^{*}+(s_{13}s_{23}^{*}-s_{14}s_{24}^{*})s_{34}^{*}+s_{23}^{*}s_{14}s_{44}^{*}\} \quad \text{(I-6a)}$$

(I-2d) and (I-2e):

$$s_{22}=\frac{1}{s_{13}^{*}s_{24}^{*}-s_{23}^{*}s_{14}^{*}}\{s_{23}s_{14}^{*}s_{33}^{*}-(s_{13}^{*}s_{23}-s_{14}^{*}s_{24})s_{34}^{*}-s_{13}^{*}s_{24}s_{44}^{*}\} \quad \text{(I-6b)}$$

(I-2b) and (I-2d):

$$s_{33}=\frac{1}{(s_{13}^{*}s_{24}^{*}-s_{23}^{*}s_{14}^{*})}\{-s_{13}s_{24}^{*}s_{11}^{*}+(s_{13}s_{14}^{*}-s_{23}s_{24}^{*})s_{12}^{*}+s_{23}s_{14}^{*}s_{22}^{*}\} \quad \text{(I-6c)}$$

(I-2c) and (I-2e):

$$s_{44}=\frac{1}{(s_{13}^{*}s_{24}^{*}-s_{23}^{*}s_{14}^{*})}\{s_{23}^{*}s_{14}s_{11}^{*}-(s_{13}^{*}s_{14}-s_{23}^{*}s_{24})s_{12}^{*}-s_{13}^{*}s_{24}s_{44}^{*}\} \quad \text{(I-6d)}$$

(I-2b), (I-2c), (I-2d) and (I-2e):

$$s_{12} = \frac{1}{2(s_{13}^{*}s_{24}^{*}-s_{23}^{*}s_{14}^{*})}\{(s_{13}s_{14}^{*}-s_{23}s_{24}^{*})s_{33}^{*}$$

$$+[(|s_{23}|^{2}-|s_{13}|^{2})-(|s_{24}|^{2}-|s_{14}|^{2})]s_{34}^{*}-(s_{13}^{*}s_{14}-s_{23}^{*}s_{24})s_{44}^{*}\} \quad \text{(I-6e)}$$

and,

$$s_{34} = \frac{1}{2(s_{13}^{*}s_{24}^{*}-s_{23}^{*}s_{14}^{*})}\{-(s_{13}s_{23}^{*}-s_{14}s_{24}^{*})s_{11}^{*}$$

$$-[(|s_{23}|^{2}-|s_{13}|^{2})-(|s_{24}|^{2}-|s_{14}|^{2})]s_{12}^{*}+(s_{13}^{*}s_{23}-s_{14}^{*}s_{24})s_{22}^{*}\} \quad \text{(I-6f)}$$

SYMMETRY REDUCTION FOR THE IDEAL SYMMETRICAL CASE

If it is assumed that the design is geometrically symmetric, i.e. the E and H arms have a common symmetric plane about which the transformation planes 1 and 2 are symmetrically spaced and that no dents or obstacles are perturbing the fields in the junction, the following symmetry conditions must be satisfied

$$s_{22} = s_{11} = |s_{11}| \exp j\phi_{11} \tag{I-7a}$$

$$s_{23} = s_{13} = |s_{13}| \exp j\phi_{13} \left[\begin{matrix}\text{H arms coupling} \\ \text{in phase}\end{matrix}\right] \tag{I-7b}$$

$$s_{24} = -s_{14} = -|s_{14}| \exp j\phi_{14} \left[\begin{matrix}\text{E arms coupling} \\ \text{in anti-phase}\end{matrix}\right] \tag{1-7c}$$

$$s_{12} = |s_{12}| \exp j\phi_{12} \quad , \quad s_{33} = |s_{33}| \exp j\phi_{33}$$

$$\text{and} \quad s_{44} = |s_{44}| \exp j\phi_{44}$$

Substituting (I-7) into (I-6f) and (I-5d) results in the decoupling constraint $s_{34} = 0$ and thus the unitarity identities reduce to

$$|s_{11}|^2 + |s_{12}|^2 + |s_{13}|^2 + |s_{14}|^2 = 1 \tag{I-8a}$$

$$\overset{*}{s}_{11}s_{12} + \overset{*}{s}_{12}s_{11} + |s_{13}|^2 - |s_{14}|^2 = 0 \tag{I-8b}$$

$$(\overset{*}{s}_{11} + \overset{*}{s}_{12})s_{13} + \overset{*}{s}_{13}s_{33} = 0 \tag{I-8c}$$

$$(\overset{*}{s}_{11} - \overset{*}{s}_{12})s_{14} + \overset{*}{s}_{14}s_{44} = 0 \tag{I-8d}$$

$$2\ |s_{13}|^2 + |s_{33}|^2 = 1 \tag{I-8e}$$

$$2\ |s_{14}|^2 + |s_{44}|^2 = 1 \tag{I-8f}$$

and similarly equations (I-6) result in

$$s_{11} = s_{22} = -\tfrac{1}{2}\left\{\overset{*}{s}_{33}\frac{s_{13}}{\overset{*}{s}_{13}} + \overset{*}{s}_{44}\frac{s_{14}}{\overset{*}{s}_{14}}\right\} \tag{I-9a}$$

$$s_{12} = -\tfrac{1}{2}\left\{\overset{*}{s}_{33}\frac{s_{13}}{\overset{*}{s}_{13}} - \overset{*}{s}_{44}\frac{s_{14}}{\overset{*}{s}_{14}}\right\} \tag{I-9b}$$

Employing the triangle in-equality

$$\Big||a|-|b|\Big| \leq |a\pm b| \leq \Big||a|+|b|\Big| \quad ,$$

it follows from (I-8c) and (I-8d) that

$$\left| \frac{|s_{33}|}{2} - \frac{|s_{44}|}{2} \right| \leq |s_{11}| \leq \left| \frac{|s_{33}|}{2} + \frac{|s_{44}|}{2} \right| \qquad \text{(I-9c)}$$

and

$$\left| \frac{|s_{33}|}{2} - \frac{|s_{44}|}{2} \right| \leq |s_{12}| \leq \left| \frac{|s_{33}|}{2} + \frac{|s_{44}|}{2} \right| \qquad \text{(I-9d)}$$

which are very useful relationships for rechecking measurement data.

Since the internal reflection coefficients s_{11}, s_{33} and s_{44} can be measured more accurately than the transformation coefficients s_{12}, s_{13} and s_{14}, the relevant phase constraints are expressed in terms of the modulus and the phase of s_{11}, s_{33} and s_{44}.

The phase of

$$s_{12} = |s_{12}|\exp j\phi_{12} = \left|\tfrac{1}{2}(|s_{33}|^2+|s_{44}|^2)-|s_{11}|^2\right|^{\frac{1}{2}}\exp j\phi_{12}$$

is defined from (I-8b) with (I-8a), (I-8e) and (I-8f) by

$$\cos(\phi_{11}-\phi_{12}) = \frac{|s_{33}|^2 - |s_{44}|^2}{4|s_{11}|\cdot[\frac{1}{2}|s_{33}|^2+\frac{1}{2}|s_{44}|^2-|s_{11}|^2]^{\frac{1}{2}}} \qquad \text{(I-10a)}$$

The phase factors ϕ_{13} and ϕ_{14} can be determined from (I-8c) and (I-8d) with (I-10a) as:

$$\tan(2\phi_{13}-\phi_{33}) = \frac{|s_{11}|\sin\phi_{11}+|s_{12}|\sin\phi_{12}}{|s_{11}|\cos\phi_{11}+|s_{12}|\cos\phi_{12}} = [s_{11},s_{12}]^{+} \qquad \text{(I-10b)}$$

$$\tan(2\phi_{14}-\phi_{44}) = \frac{|s_{11}|\sin\phi_{11}-|s_{12}|\sin\phi_{12}}{|s_{11}|\cos\phi_{11}-|s_{12}|\cos\phi_{12}} = [s_{11},s_{12}]^{-} \qquad \text{(I-10c)}$$

Thus

$$\theta_{13} = (2\phi_{13}-\phi_{33}) = \text{arc tan } [s_{11},s_{12}]^{+} = \text{const.} \qquad \text{(I-10d)}$$

$$\theta_{14} = (2\phi_{14}-\phi_{44}) = \text{arc tan } [s_{11},s_{12}]^{-} = \text{const.} \qquad \text{(I-10e)}$$

The interrelated phase constraint of all the six scattering parameters is obtained from (I-9a) and (I-9b), where with (I-10)

$$2|s_{11}|\exp j\phi_{11} = -\{|s_{33}|\exp j\theta_{13}+|s_{44}|\exp j\theta_{14}\} \qquad \text{(I-11a)}$$

$$2|s_{12}|\exp j\phi_{12} = -\{|s_{33}|\exp j\theta_{13}-|s_{44}|\exp j\theta_{14}\} \qquad \text{(I-11b)}$$

Subtracting the squared moduli of these equations yields

$$\cos(\theta_{13}-\theta_{14}) = \frac{2|s_{11}|^2-\frac{1}{2}|s_{33}|^2-\frac{1}{2}|s_{44}|^2}{|s_{33}||s_{44}|} \qquad \text{(I-12a)}$$

Multiplying (I-11a) by the complex conjugate of (I-11b) and equating the real and imaginary parts, results in (I-10a) and

$$\sin(\theta_{14}-\theta_{13}) = \frac{2|s_{11}|\cdot|\frac{1}{2}(|s_{33}|^2+|s_{44}|^2)-|s_{11}|^2|^{\frac{1}{2}}\cdot\sin(\phi_{11}-\phi_{12})}{|s_{33}||s_{44}|} \qquad \text{(I-12b)}$$

and therefore

$$\tan(\theta_{14}-\theta_{13}) = \frac{2|s_{11}|\cdot|\frac{1}{2}(|s_{33}|^2+|s_{44}|^2)-|s_{11}|^2|^{\frac{1}{2}}\cdot\sin(\phi_{11}-\phi_{12})}{|2|s_{11}|^2-\frac{1}{2}(|s_{33}|^2+|s_{44}|^2)|}$$

$$= [s_{11},\ s_{12}] \qquad \text{(I-12c)}$$

or

$$(\theta_{14}-\theta_{13}) = \text{arc tan } [s_{11},\ s_{12}]$$

where ϕ_{12} is determined by (I-10a) and thus $(\theta_{14}-\theta_{13})$ is indeterminate by a factor of π. However, according to (I-9), all phase angles can otherwise be uniquely determined.

SYMMETRY REDUCTION FOR THE SLIGHTLY ASYMMETRICAL CASE

Inspecting the symmetry constraints of (I-5) and (I-6), it is obvious that a simplified closed form solution cannot be given for the general asymmetrical design case. Therefore for purposes of error analysis, the first order perturbations from the ideally symmetric case are considered only where the scattering coefficients are denoted by $\sigma_{\mu\nu}$. Coupling is encountered whenever

$$\sigma_{33} \neq \sigma_{44} \neq 0 \quad , \quad \sigma_{11} \neq \sigma_{22} \neq 0$$

and

$$\sigma_{23} \neq \sigma_{13} \quad , \quad \sigma_{24} \neq -\sigma_{14}$$

Therefore, it is logical to treat the slightly asymmetrical mismatched case for

$$|\sigma_{23}| = |\sigma_{13}| \quad \text{and} \quad |\sigma_{24}| = |\sigma_{14}| \qquad \text{(I-13a)}$$

so that

$$\begin{aligned} \sigma_{13} &= s_{13}\exp j\delta_{13} \quad , \quad & \sigma_{23} &= s_{13}\exp -j\delta_{13} \\ \sigma_{14} &= s_{14}\exp j\delta_{14} & \sigma_{24} &= -s_{14}\exp -j\delta_{14} \end{aligned} \qquad \text{(3.2.1a)}$$

and thus from (I-5a)

$$|\sigma_{11}|^2 - |\sigma_{22}|^2 = 0 \qquad \text{(I-13b)}$$

and from (I-4b) and (I-4e)

$$|\sigma_{33}|^2 = |s_{33}|^2 - |\sigma_{34}|^2 \quad , \quad |\sigma_{44}|^2 = |s_{44}|^2 - |\sigma_{34}|^2$$

where

$$\sigma_{11} = -\tfrac{1}{2}\{\frac{s_{13}}{s_{13}^*}\sigma_{33}^* + \frac{s_{14}}{s_{14}^*}\sigma_{44}^*\}\ \frac{[|s_{13}|^2\exp+j2\delta_{13} - |s_{14}|^2\exp+2j\delta_{14}]}{(|s_{13}|^2 - |s_{14}|^2)} \qquad \text{(I-13c)}$$

$$\sigma_{12} = -\tfrac{1}{2}\{\ \frac{s_{13}}{s_{13}^*}\ \sigma_{33}^* - \frac{s_{14}}{s_{14}^*}\ \sigma_{44}^*\} \qquad \text{(I-13d)}$$

$$\sigma_{22} = -\tfrac{1}{2}\{\frac{s_{13}}{s_{13}^*}\sigma_{33}^* + \frac{s_{14}}{s_{14}^*}\sigma_{44}^*\}\ \frac{[|s_{13}|^2\exp-j2\delta_{13} - |s_{14}|^2\exp-2j\delta_{14}]}{(|s_{13}|^2 - |s_{14}|^2)} \qquad \text{(I-13e)}$$

$$\sigma_{34} = \frac{j\ \sin(\delta_{13}-\delta_{14})}{(|s_{13}|^2-|s_{14}|^2)}\ (s_{13}^*s_{14}\sigma_{33}+s_{13}s_{14}^*\sigma_{44}) \qquad \text{(I-13f)}$$

or

$$\sigma_{33} = -\frac{s_{13}}{s_{13}^*}\{\frac{(\sigma_{11}^*+\sigma_{22}^*)}{2}\ \frac{[|s_{13}|^2 - |s_{14}|^2]}{[|s_{13}|^2\cos2\delta_{13} - |s_{14}|^2\cos2\delta_{14}]} + \sigma_{12}^*\} \qquad \text{(I-14a)}$$

$$\sigma_{34} = -\frac{j\ \sin(\delta_{13}-\delta_{14})s_{13}s_{14}(\sigma_{11}^*+\sigma_{22}^*)}{2[|s_{13}|^2\cos2\delta_{13} - |s_{14}|^2\cos2\delta_{14}]} \qquad \text{(-14b)}$$

$$\sigma_{44} = -\frac{s_{14}}{s_{14}^*}\{\ \frac{(\sigma_{11}^*+\sigma_{22}^*)}{2}\ \ \frac{[|s_{13}|^2 - |s_{14}|^2]}{[|s_{13}|^2\cos2\delta_{13} - |s_{14}|^2\cos2\delta_{14}]} - \sigma_{12}^*\} \qquad \text{(I-14c)}$$

Inspecting the expressions of (I-13) and (I-14), it can be assumed that

$$\sigma_{12} = s_{12} \quad , \quad \sigma_{11} = s_{11}\exp+j\delta_{11} \quad , \quad \sigma_{22} = s_{11}\exp-j\delta_{11} \qquad \text{(3.5b)}$$

and thus for $\sigma_{13} \neq \sigma_{14}$

$$\sigma_{34} = \frac{-j\ \sin(\delta_{13}-\delta_{14})\cos\delta_{11} s_{13} s_{14} s_{11}^{*}}{[|s_{13}|^2\cos 2\delta_{13}-|s_{14}|^2\cos 2\delta_{14}]} \tag{I-15a}$$

where

$$\exp 2j\delta_{11} = \frac{|s_{13}|^2\exp{+2j\delta_{13}}-|s_{14}|^2\exp{+j2\delta_{14}}}{|s_{13}|^2\exp{-2j\delta_{13}}-|s_{14}|^2\exp{-j2\delta_{14}}}$$

which when simplified gives

$$\delta_{11} = \tan^{-1}\left\{\frac{|s_{13}|^2\sin(2\delta_{13})-|s_{14}|^2\sin(2\delta_{14})}{|s_{13}|^2\cos(2\delta_{13})-|s_{14}|^2\cos(2\delta_{14})}\right\} \tag{I-15b}$$

and σ_{33} and σ_{44} change in amplitude and phase

$$\sigma_{33} = -\frac{s_{13}}{s_{13}^{*}}\left\{\frac{s_{11}^{*}[|s_{13}|^2-|s_{14}|^2]\cos\delta_{11}}{[|s_{13}|^2\cos 2\delta_{13}-|s_{14}|^2\cos 2\delta_{14}]} + \sigma_{12}^{*}\right\} \tag{I-15c}$$

$$|\sigma_{33}|^2 = |s_{33}|^2 - |\sigma_{34}|^2$$

and

$$\sigma_{44} = -\frac{s_{14}}{s_{14}^{*}}\left\{\frac{s_{11}^{*}[|s_{13}|^2-|s_{14}|^2]\cos\delta_{11}}{[|s_{13}|^2\cos 2\delta_{13}-|s_{14}|^2\cos 2\delta_{14}} + \sigma_{12}^{*}\right\} ,$$

$$|\sigma_{44}|^2 = |s_{44}|^2 - |\sigma_{34}|^2 \tag{I-15d}$$

APPENDIX II

THE TRANSFORMATION LOCI

To derive the transformation equations of the circular loci $L_3(\psi_3 = \text{const.}, \psi_4 = \text{adjustable})$ and $L_4(\psi_4 = \text{const.}, \psi_3 = \text{adjustable})$, it is found convenient to relate the polar plane of the complex reflection coefficient $\Gamma = |\Gamma| \exp j\psi$ to the Argand plane as shown in Fig.13a, where

$$\Gamma = |\Gamma| \exp j\psi = u + jv \tag{II-1a}$$

The equation of a circular locus which intersects the origin $\Gamma = 0$, is tangent to the mismatch circle $|\Gamma| = 1$, and is characterized by the total transformation angle ψ_f for a fixed stub length, is given by

$$(u - \tfrac{1}{2}\cos\psi_f)^2 + (v - \tfrac{1}{2}\sin\psi_f)^2 = 1/4 \tag{II-1b}$$

where ψ_f is defined in the positive mathematical sense as shown in Figs. 13a and 13b, and u and v depend on the adjustable stub lengths of the complementary arm.

Thus the equations of the circular loci L_3 and L_4, as shown in Fig. 13b, are given by

$$L_3(\psi_3 = \text{const.}) : \Gamma_3^2 = u_3^2 + v_3^2 = u_3\cos\psi_3 + v_3\sin\psi_3 \tag{II-2a}$$

$$L_4(\psi_4 = \text{const.}) : \Gamma_4^2 = u_4^2 + v_4^2 = u_4\cos\psi_4 + v_4\sin\psi_4 \tag{II-2b}$$

where $u_3 = u_3(\psi_4)$, $v_3 = v_3(\psi_4)$ and $u_4 = u_4(\psi_3)$

$$v_4 = v_4(\psi_3)$$

The intersection point L_3 and L_4, which defines the reflection coefficient

$$\Gamma = s_{22} = |\Gamma| \exp j\psi,$$

is defined by

$$\Gamma_3(\psi_4) = \Gamma_4(\psi_3) = \Gamma(\psi_3,\psi_4) \quad \text{or}$$

$$\begin{aligned} u_3(\psi_4) &= u_4(\psi_3) = u(\psi_3,\psi_4) \\ v_3(\psi_4) &= v_4(\psi_3) = v(\psi_3,\psi_4) \end{aligned} \tag{II-2c}$$

so that,

$$u(\cos\psi_3 - \cos\psi_4) = v(\sin\psi_4 - \sin\psi_3) \tag{II-2d}$$

The argument of the reflection coefficient associated with (II-2c) is then obtained from (II-2d) as

$$\tan\psi = \frac{v}{u} = \tan\left(\frac{\psi_3+\psi_4}{2}\right) \tag{II-3a}$$

Eliminating u and v for $\Gamma_3 = \Gamma_4 = \Gamma$ in (II-2a) and (II-2b) yields

$$|\Gamma|^2 = \cos^2\left(\frac{\psi_3-\psi_4}{2}\right) \tag{II-3b}$$

Since $|\Gamma|$ defines the absolute value of the radius vector in the polar reflection coefficient plane, Γ is defined by the intersection point of two circular transformation loci L_3 and L_4, where

$$\Gamma = |\Gamma| \exp j\psi = \pm\cos\left(\frac{\psi_3-\psi_4}{2}\right) \exp j\left(\frac{\psi_3+\psi_4}{2}\right)$$

which uniquely specifies the matching procedures.

It is thus shown that the loadside reflection coefficient $\Gamma_2^* = s_{22}$ as defined in equation (3.1.4) does indeed represent the analytical expression of two intersecting circular loci $L_3(\psi_3 = \text{const.},$

ψ_4 = adjustable) and $L_4(\psi_4$ = const., ψ_3 = adjustable). However, it is to be noted that the adjustable transformation angles do not, in general, represent the tunable electric stub lengths $\phi_3 = \beta\ell_3$ and $\phi_4 = \beta\ell_4$, which is evident from (3.1.3) and (3.1.4).

If the E-H tuners are to be employed as automated, self-controllable conjugate impedance matching devices, it is found useful to derive a procedure of determining $\cos\psi_3$, $\cos\psi_4$, $\sin\psi_3$, and $\sin\psi_4$ only in terms of $|\Gamma|^2$ and $\tan\psi$ which are obtained from s_{22}, if the proper equivalent circuit of the microwave junction is synthesized. Such explicit expressions in terms of ψ_3 and ψ_4 can straightforwardly be obtained by employing trigonometric expansions in (II-2) and (II-3) and formulating

$$\alpha = \cos\psi_3\cos\psi_4 = (|\Gamma|^2-1) + \frac{1}{1+\tan^2\psi} \tag{II-4a}$$

$$\beta = \sin\psi_3\sin\psi_4 = |\Gamma|^2 - \frac{1}{1-\tan^2\psi} \tag{II-4b}$$

$$\nu_{\pm(-)} = \sin\psi_3\cos\psi_4 = \frac{\tan\psi}{1+\tan^2\psi} \pm \sqrt{|\Gamma|^2(1-|\Gamma|^2)} \tag{II-4c}$$

$$\delta_{\pm(-)} = \cos\psi_3\sin\psi_4 = \frac{\tan\psi}{1+\tan^2\psi} \mp \sqrt{|\Gamma|^2(1-|\Gamma|^2)} \tag{II-4d}$$

$$[\alpha\beta - \nu_{\pm(-)}\,\delta_{\pm(-)}] = 0 \tag{II-4e}$$

It is to be noted that the ambiguity of defining a positive or negative root in (II-4c) and (II-4d) indicates that two pairs of solutions exist as verified earlier. Thus explicit expressions for

$\tan\psi_3$ and $\tan\psi_4$ are obtained, where

$$\tan\psi_{3+} = \frac{\nu_+}{\alpha} = \frac{\beta}{\delta_+} \quad , \quad \tan\psi_{3-} = \frac{\delta_-}{\alpha} = \frac{\beta}{\nu_-} \qquad \text{(II-5a)}$$

or

$$\tan\psi_{4+} = \frac{\delta_+}{\alpha} = \frac{\beta}{\nu_+} \quad , \quad \tan\psi_{4-} = \frac{\nu_-}{\alpha} = \frac{\beta}{\delta_-} \qquad \text{(II-5b)}$$

For the properly synthesized equivalent circuit of a lossless, reciprocal E-H tuner whose E and H arms are perfectly decoupled, the resulting expression of $\tan\psi_3$ can only depend on $\phi_4 = \beta\ell_4$, [since $\psi_3 = f(\phi_3 = \text{const.}, \phi_4 = \text{adjustable})$] and that of $\tan\psi_4$ can only depend on $\phi_3 = \beta\ell_3$. [Since $\psi_4 = f(\phi_4 = \text{const.}, \phi_3 = \text{adjustable})$]. Otherwise the measurement results of Figs. 6a and 6b cannot be satisfied.

ELLIPTICAL TRANSFORMATION LOCI

Since experimental results obtained for the slightly asymmetrical case indicated that the circular loci degenerate into elliptical loci whose minor axis is the polar radius vector ($|\Gamma|$) in the Argand plane, the transformation equations for slightly elliptical loci are derived for the purpose of error analysis.

The general equation of an ellipse of eccentricity ε, which intersects the matching point $\Gamma = 0$, is tangent to the mismatch circle $\Gamma = 1$, and whose minor (or major axis) is inclined by an angle ψ^ε with the positive real axis u in the Argand plane, is given by

$$\frac{1}{a^2} f(u,v,\varepsilon,\psi^\varepsilon) = \{(1-\varepsilon^2\cos^2\psi^\varepsilon)u^2 - 2\varepsilon^2\cos\psi^\varepsilon\sin\psi^\varepsilon uv + (1-\varepsilon^2\sin^2\psi^\varepsilon)$$

$$v^2-(1-\varepsilon^2)\cos\psi^\varepsilon\cdot u-(1-\varepsilon^2)\sin\psi^\varepsilon\cdot v\} \equiv 0 \qquad \text{(II-6a)}$$

where a is the major axis, $e^2 = a^2 - b^2$, and $\varepsilon = e/a$ is the numerical excentricity. It is to be noted that $-\frac{1}{2} < |\varepsilon|^2 < \frac{1}{2}$, where for:

$-\frac{1}{2} < \lvert\varepsilon\rvert^2 < 0$	elliptical loci with minor axis parallel to radiant vector
$\lvert\varepsilon\rvert^2 = 0$	circular loci
$0 < \lvert\varepsilon\rvert^2 < \frac{1}{2}$	elliptical loci with major axis parallel to radiant vector

Employing similar procedures of evaluation it can be shown that

$$\Gamma_\varepsilon = \frac{\cos\left(\frac{\psi_3^\varepsilon-\psi_4^\varepsilon}{2}\right)\exp\ j\left(\frac{\psi_3^\varepsilon+\psi_4^\varepsilon}{2}\right)}{\left[1+\frac{\varepsilon^2}{1-\varepsilon^2}\sin^2\left(\frac{\psi_3^\varepsilon-\psi_4^\varepsilon}{2}\right)\right]} \qquad \text{(II-6c)}$$

represents the reflection coefficient in terms of the intersecting elliptical loci ψ_3^ε (ψ_4^ε adjustable) = const. and ψ_4^ε (ψ_3^ε adjustable) = const. as is shown in Fig. 13c.

APPENDIX III

COMPUTER PROGRAM FOR COMPUTION OF TRANSFORMATION LOCI OF EQN (3.2.2) AND RELATED DISCUSSION

For the purpose of the verification of the closed form solution (3.1.4c), the transformation loci are computed for the asymmetric E-H junction using eqn (3.2.2a) and (3.2.2b). The plot thus obtained is then compared with the loci, obtained from experimentally measured data, to verify the authenticity of the solution. Because of the limitations imposed by the available equipments, it was not possible to fabricate an E-H junction, accurately, with desired asymmetries. This forbids the checking of measured data, point by point with the computed data, hence only the general shape of the transformation loci (inside the unit mismatch circle) will be verified.

EQUATIONS AND BLOCK DIAGRAM OF PROGRAM

The equations to be calculated are (3.2.2.a) and (3.2.2b)

Input available (assumed) are,

$$s_{11} = |s_{11}|\exp(j\phi_{11}) = 0.3\ \exp(j60°)$$

$$s_{33} = |s_{33}|\exp(j\phi_{33}) = 0.4\ \exp(j15°)$$

$$s_{44} = |s_{44}|\exp(j\phi_{44}) = 0.6\ \exp(j205°)$$

and $s_{14} = -s_{13} = 1°$

For computing $|s_{12}|$ and ϕ_{12}, (I-8a) and (I-10a) has been used.

$$|s_{12}| = [1-|s_{11}|^2 - (|s_{13}|^2 + |s_{14}|^2)]^{1/2}$$

$$= [\frac{|s_{33}|^2 + |s_{44}|^2}{2} - |s_{11}|^2]^{1/2}$$

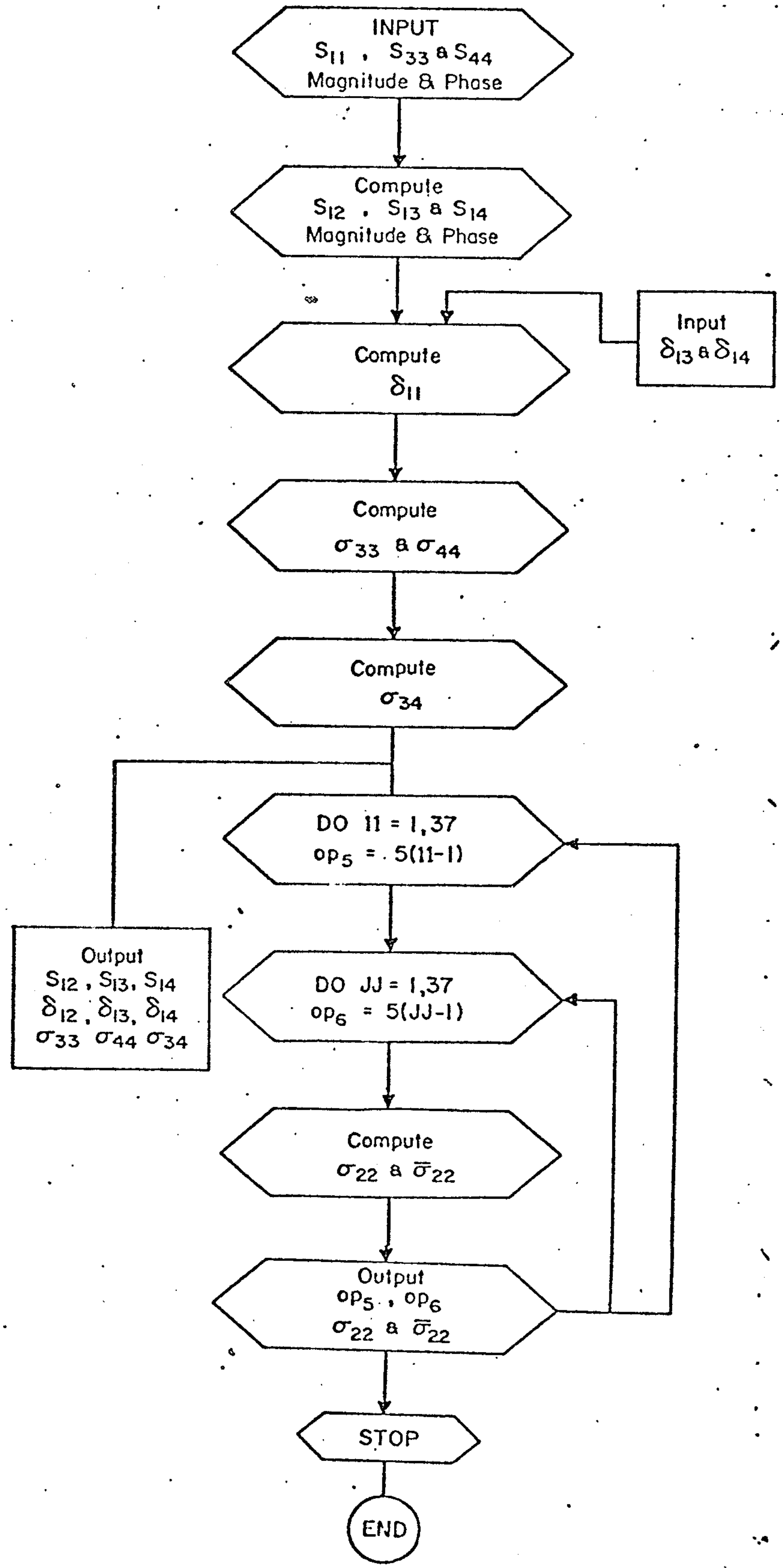

FIG. 18 BLOCK DIAGRAM OF COMPUTER PROGRAM

Because,

$$2|s_{13}|^2 + |s_{33}|^2 = 1 \qquad \text{(I-8e)}$$

$$2|s_{14}|^2 + |s_{44}|^2 = 1 \qquad \text{(I-8f)}$$

(I-8e) and (I-8f) were also used to calculate the magnitude of s_{13} and s_{14} respectively. The phase of s_{13} and s_{14} were obtained by using (I-10b) and (I-10c) respectively. Next s_{11} was computed by using (I-15b). σ_{33} and σ_{44} were computed using (I-15c) and (I-15d) respectively. It assumed that $s_{12} = \sigma_{12}$. Fig. 18., shows the block diagram of the computation.

COMPUTER PROGRAM

```
$JOB    WATFIV
        COMPLEX Z11
        COMPLEX CONJG
        COMPLEX CMPLX,PD33,PD44,FD33,FD44,SIG33,SIG44,CEXP,SIG34,EF55
        COMPLEX EF66,YUS,DINO,DINV,S11,XE11,XE13,XE14,XE,S13,S14,Z1,Z2,Z3
        COMPLEX Z4,SIG22,PLX,W1,W2,W3,W4,W11,SGB22
        COMPLEX S,APH11,APH13,APH14,APH
        S=CMPLX(0.,1.0)
        R=2*3.14/360
        WGS11=0.3
        WGS33=0.4
        WGS44=0.6
        PHI11=60*R
        PHI33=15*R
        PHI44=205*R
        SWS12=0.5*(WGS33*WGS33+WGS44*WGS44)-WGS11*WGS11
        WGS12=SQRT(SWS12)
        SWS13=0.5*(1.0-WGS33*WGS33)
        WGS13=SQRT(SWS13)
        SWS14=0.5*(1.0-WGS44*WGS44)
        WGS14=SQRT(SWS14)
        PHI12=(WGS33*WGS33-WGS44*WGS44)/(4*WGS11*WGS12)
        P1112=ARCOS(PHI12)
        PHI12=PHI11-P1112
        UP3=WGS11*SIN(PHI11)+WGS12*SIN(PHI12)
        DOWN3=WGS11*COS(PHI11)+WGS12*CCS(PHI12)
        UP4=WGS11*SIN(PHI11)-WGS12*SIN(PHI12)
        DOWN4=WGS11*COS(PHI11)-WGS12*CCS(PHI12)
```

```
      P1333=ATAN2(UP3,DOWN3)
      P1444=ATAN2(UP4,DOWN4)
      PHI13=0.5*(PHI33+P1333)
      PHI14=0.5*(PHI44+P1444)
      DEL13=1.0*R
      DEL14=-DEL13
      UP1=WGS13*WGS13*SIN(2*DEL13)-WGS14*WGS14*SIN(2*DEL14)
      DOWN1=WGS13*WGS13*COS(2*DEL13)-WGS14*WGS14*COS(2*DEL14)
      DEL11=ATAN2(UP1,DOWN1)
      X11=WGS11*COS(PHI11)
      Y11=WGS11*SIN(PHI11)
      S11=CMPLX(X11,Y11)
      APH11=(-DEL11)*S
      APH13=(-2*DEL13)*S
      APH14=(-2*DEL14)*S
      APH=-(DEL13+DEL14)*S
      XE11=CEXP(APH11)
      XE13=CEXP(APH13)
      XE14=CEXP(APH14)
      XE=CEXP(APH)
      X13=WGS13*COS(PHI13)
      Y13=WGS13*SIN(PHI13)
      X14=WGS14*COS(PHI14)
      Y14=WGS14*SIN(PHI14)
      S13=CMPLX(X13,Y13)
      S14=CMPLX(X14,Y14)
      A1=WGS11*COS(PHI11)*(WGS13*WGS13-WGS14*WGS14)*COS(DEL11)/(WGS13*WG
     1S13*COS(2*DEL13)-WGS14*WGS14*COS(2*DEL14))
      B1=WGS11*SIN(PHI11)*(WGS13*WGS13-WGS14*WGS14)*COS(DEL11)/(WGS13*WG
     2S13*COS(2*DEL13)-WGS14*WGS14*COS(2*DEL14))
      AA1=-(A1+WGS12*COS(PHI12))
      BB1=B1+WGS12*SIN(PHI12)
      AA2=-A1+WGS12*COS(PHI12)
      BB2=B1-WGS12*SIN(PHI12)
      PD33=CMPLX(AA1,BB1)
      PD44=CMPLX(AA2,BB2)
      FD33=S13/CONJG(S13)
      FD44=S14/CONJG(S14)
      SIG33=FD33*PD33
      SIG44=FD44*PD44
      X33=REAL(SIG33)
      Y33=AIMAG(SIG33)
      X44=REAL(SIG44)
      Y44=AIMAG(SIG44)
      DEL=DEL13-DEL14
      PHI=PHI13+PHI14-PHI11
      X34=(WGS13*WGS14*SIN(DEL)*WGS11*COS(DEL11)*SIN(PHI))/DOWN1
      Y34=-(WGS13*WGS14*SIN(DEL)*WGS11*COS(DEL11)*COS(PHI))/DOWN1
      SIG34=CMPLX(X34,Y34)
      WRITE(6,100) WGS12,PHI12, WGS13, PHI13, WGS14, PHI14
  100 FORMAT(1H0,5X,'S12=',F6.4,'<',F8.3,10X,'S13=',F6.4,'<',F8.3,10X,'S
     3S14=',F6.4,'<',F8.3)
```

```
      WRITE(6,101) DEL13, DEL14, DEL11
101   FORMAT(1H0,10X,'DEL13=',F7.3,10X,'DEL14=',F7.3,10X,'DEL11=',F7.3)
      WRITE(6,102) X33, Y33, X44, Y44, X34, Y34
102   FORMAT(1H0,10X,'SIGMA33=',F10.5,',',F10.5,10X,'SIGMA44=',F10.5,','
     4,F10.5,10X,'SIGMA34=',F10.5,',',F10.5)
      WRITE(6,104)
104   FORMAT(1H0,5X,'RE(S22)',6X,'IM(S22)',8X,'MAG',8X,'ANG(S22)',5X,'R(
     5SB22)',6X,'IM(SB22)',5X,'MAG(SB22)',4X,'ANG(SB22)',4X,'PHI3',6X,'P
     6HI4')
      DO 2 II=1,37
      DO 3 JJ=1,37
      PHI3=5*(II-1)*R
      PHI4=5*(JJ-1)*R
      E5=-(COS(2*PHI3)+X33)
      F5=-(SIN(2*PHI3)+Y33)
      EF55=CMPLX(E5,F5)
      E6=-(COS(2*PHI4)+X44)
      F6=-(SIN(2*PHI4)+Y44)
      EF66=CMPLX(E6,F6)
      YUS=EF55*EF66
      ANT=REAL(YUS)
      BNT=AIMAG(YUS)
      DINR=ANT-(X34*X34-Y34*Y34)
      DINI=BNT-(2*X34*Y34)
      DINO=CMPLX(DINR,DINI)
      DINV=1.0/DINO
      Z1=S11*XE11*DINO
      Z2=S13*S13*XE13*EF66
      Z3=S14*S14*XE14*EF55
      Z4=2*S13*S14*XE*SIG34
      Z11=Z1+Z2+Z3-Z4
      SIG22=Z11*DINV
      X22=REAL(SIG22)
      Y22=AIMAG(SIG22)
      PHI22=ATAN2(Y22,X22)
      WGS=X22*X22+Y22*Y22
      WGS22=SQRT(WGS)
      D134=DEL13+DEL14
      SI=2*SIN(D134)
      PLX=CMPLX(0.,SI)
      W1=S11*COS(DEL11)*DINC
      W2=S13*S13*COS(2*DEL13)*EF66
      W3=S14*S14*COS(2*DEL14)*EF55
      W4=S13*S14*PLX*SIG34
      W11=W1+W2+W3+W4
      SGB22=W11*DINV
      XB22=REAL(SGB22)
      YB22=AIMAG(SGB22)
      PHB22=ATAN2(YB22,XB22)
      WGB=XB22*XB22+YB22*YB22
      WGB22=SQRT(WGB)
      PHI3=PHI3/R
```

PARAMETERS (angles in radians)

$s_{12} = 0.4123\angle -0.940$, $s_{13} = 0.6481\angle 0.039$, $s_{14} = 0.5657\angle 2.651$

$\delta_{13} = 0.017$, $\delta_{14} = -0.017$, $\delta_{11} = 0.253$

$\sigma_{33} = -0.381-j0.111$, $\sigma_{44} = 0.54+j0.244$, $\sigma_{34} = 0.037+j0.0027$

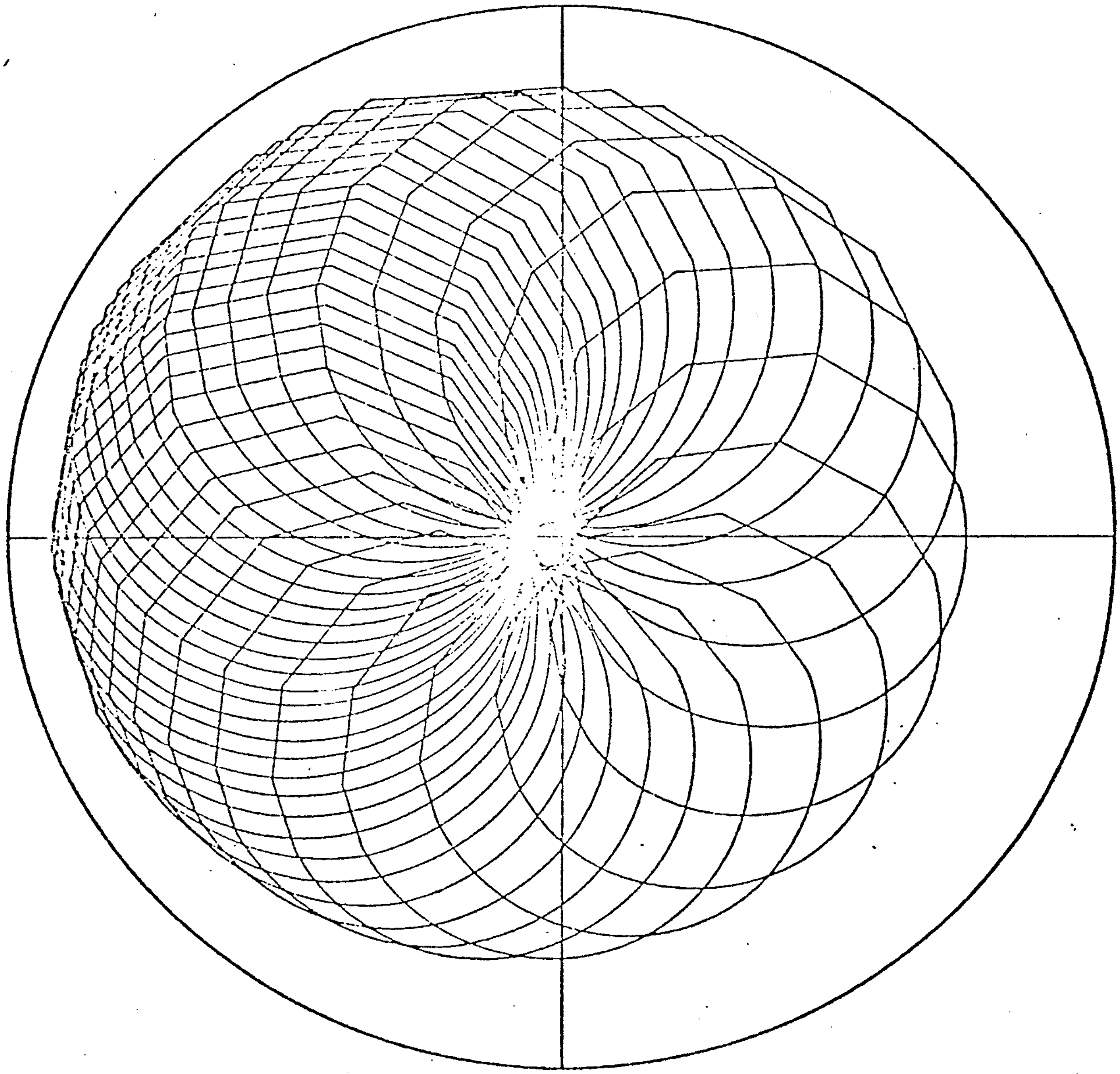

Fig. 19 THEORETICALLY DETERMINED TRANSFORMATION LOCI OF E-H TUNER

each circle corresponds to ψ_3=const , $\psi_4 \rightarrow 0$ to 180 degrees

```
      PHI4=PHI4/R
      PHI22=PHI22/R
      PHB22=PHB22/R
      WRITE(6,103) X22, Y22, WGS22, PHI22, XB22, YB22, WGB22, PHB22,PHI3
     7,PHI4
  103 FORMAT(1H0,5X,F8.3,5X,F8.3,5X,F8.3,5X,F8.3,5X,F8.3,5X,F8.3,5X,F8.3
     8,5X,F8.3,5X,F5.1,5X,F5.1)
      WRITE(7,110) WGS22, PHI22
  110 FORMAT(10X,F10.5,10X,F10.5)
    3 CONTINUE
    2 CONTINUE
      STOP
      END
```

Fig.19 shows the theoretically computed transformation loci, which could be compared with Fig. 12 for experimental verification of the theory.

DISCUSSION AND CONCLUSION

As it was pointed out earlier in this appendix, it is not convenient to check experimental results point by point with computed results. But the reverse process could provide a means for measuring the asymmetry in fabricated junctions. Theoretically transformation loci can be plotted for all possible values of s_{13} and s_{14}. The experimentally plotted transformation loci of the junction could be compared with these theoretical plots to obtain a first order estimate of the asymmetry of the junction, (asymmetry in phase only).

Finally it is concluded that the plot of the transformation loci obtained from the measurement, [see Fig.12] do verify the closed form solution of the transformation loci of the E-H junction.